NeuroImage 253 (2022) 119110

Contents lists available at ScienceDirect

NeuroImage

journal homepage: www.elsevier.com/locate/neuroimage

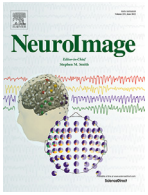

Review

Network analysis of neuroimaging in mice

Leon Scharwächter[a], Felix J. Schmitt[a,b], Niklas Pallast[a], Gereon R. Fink[a,c], Markus Aswendt[a,c,*]

[a] University of Cologne, Faculty of Medicine and University Hospital Cologne, Dept. of Neurology, Cologne, Germany
[b] University of Cologne, Institute of Zoology, Dept. of Computational Systems Neuroscience, Cologne, Germany
[c] Cognitive Neuroscience, Institute of Neuroscience and Medicine (INM-3), Research Center Juelich, Germany

ARTICLE INFO

Keywords:
DTI
rs-fMRI
Connectivity
Graph analysis
Brain network

ABSTRACT

Graph theory allows assessing changes of neuronal connectivity and interactions of brain regions in response to local lesions, e.g., after stroke, and global perturbations, e.g., due to psychiatric dysfunctions or neurodegenerative disorders. Consequently, network analysis based on constructing graphs from structural and functional MRI connectivity matrices is increasingly used in clinical studies. In contrast, in mouse neuroimaging, the focus is mainly on basic connectivity parameters, i.e., the correlation coefficient or fiber counts, whereas more advanced network analyses remain rarely used. This review summarizes graph theoretical measures and their interpretation to describe networks derived from recent in vivo mouse brain studies. To facilitate the entry into the topic, we explain the related mathematical definitions, provide a dedicated software toolkit, and discuss practical considerations for the application to rs-fMRI and DTI. This way, we aim to foster cross-species comparisons and the application of standardized measures to classify and interpret network changes in translational brain disease studies.

Introduction

The brain is a complex dynamic system that comprises many different structures interacting as functional units with nonrandom topological features in a large-scale network (Sporns and Bullmore, 2014). Among the non-invasive imaging techniques with an apparent translational component, MRI provides non-invasive access to functional and structural details of that network using sequences such as Diffusion Tensor Imaging (DTI) and resting-state functional MRI (rs-fMRI). In humans, these approaches helped to better characterize individual variability and behavioral performance, to identify biomarkers of acute and neurodegenerative diseases (Grefkes and Fink, 2014; Andica et al., 2019), and to select targets for neuromodulation (Horn and Fox, 2020). The recent advent of small animal-specific MRI hardware and sequences optimized to small rodent brains allows urgently needed complementary studies of the basic concepts of neural processing and associated connectivity changes (Hoehn and Aswendt, 2013; Pan et al., 2015; Müller et al., 2020), and the network effects related to spontaneous and therapy-induced behavioral improvement after brain disease (Harsan et al., 2013; Jonckers et al., 2015; Green et al., 2018; Aswendt, Pallast, et al., 2020; Blaschke et al., 2021).

According to the conventional region-by-region connectivity analysis, a small number of regions is selected for a detailed subnetwork analysis. This approach is biased for the brain regions selected and underrepresents the breadth and detail of whole-brain connectivity data. Here, a network approach using graph theory has been proven helpful in clinical/human MRI (reviewed, e.g., in (Sporns, 2010; Fallani et al., 2014; Hallquist and Hillary, 2018; Farahani et al., 2019)). The critical advantage of this approach is that it allows assessing far-distance interactions and network alterations in generalized local and global network measures, which can be directly compared between studies and embedded in more general network models of health and disease (Bullmore and Sporns, 2009; Sporns, 2010; van den Heuvel and Sporns, 2019), e.g., stroke or Alzheimer's disease (Crofts et al., 2011; Stam et al., 2006). For this purpose, the mouse model is advantageous as it offers a direct and individual correlation of network measures with cellular and molecular features. Implementing harmonized and atlas-based network measures is therefore a promising strategy to advance the interpretation of connectivity parameters in mouse brain studies.

This review introduces the essential concepts of brain network analysis and their interpretation based on mouse MR neuroimaging studies. We further share software to facilitate a new form of large-scale, multicenter, translational mouse brain studies. The overview is limited to mouse MR neuroimaging as the most widely used animal model with versatile options for genetic modifications, detailed anatomical mapping, viral tracing, and gene expression available (Hawrylycz et al., 2011; Hess et al., 2018; Lein et al., 2007; Oh et al., 2014; Wang et al., 2020). Notably, the conclusions do not exclude other small animal models and complement earlier reviews of connectivity, e.g., in the

* Corresponding author.
E-mail address: markus.aswendt@uk-koeln.de (M. Aswendt).

https://doi.org/10.1016/j.neuroimage.2022.119110.
Received 17 December 2021; Received in revised form 1 March 2022; Accepted 15 March 2022
Available online 17 March 2022.

rat brain (Bifone et al., 2010) and in clinical studies (Hallquist and Hillary, 2018)).

Mouse-specific requirements for imaging structural and functional connectivity

Mouse brain MRI has special hardware requirements to achieve with an approximately 2800-fold smaller brain volume the image quality comparable with human MRI. Therefore, it requires much higher magnetic field strengths to increase the signal to noise ratio while obtaining high resolution images (common voxel sizes: 100-300 μm in plane and 300-750 μm slice thickness). For both DTI and rs-fMRI, fast echo-planar imaging (EPI) based on a gradient-echo is most often used, despite the potential susceptibility artefacts, which should be minimized by careful application of strong, higher-order shims (Pan et al., 2015).

In the classical and most widely used fiber tracking experiment using Diffusion Tensor Imaging (DTI), fiber tracts are estimated and reconstructed in 3D based on the directional dependence of water diffusivity along with white matter structures (Pierpaoli and Basser, 1996). DTI has been optimized for the mouse brain to limit susceptibility- and motion-induced artifacts at ultra high fields (Boretius et al., 2007; Harsan et al., 2013; Aswendt et al., 2020). However, it remains a challenge to acquire multi-directional diffusion data with high b-values for high diffusion contrast and a sufficient signal-to-noise ratio in a reasonable scan time considering animal welfare (typically: below 1.5 hours) (Müller et al., 2020). Even under ideal experimental conditions, the choice of diffusion modeling (deterministic vs. probabilistic) and parameters (e.g. step size, cutoff values, number of streamlines) affect the tractography performance (Karatas et al., 2021). Further limitations for interpretation should be considered: i) tractography is bidirectional, not necessarily constrained by synapses, and might include multiple axons (Calabrese et al., 2015), ii) it remains challenging to resolve crossing fibers with a conventionally used low number of gradient directions (typically around 30), and iii) diffusion anisotropy might be influenced by additional tissue parameters such as level of myelination and fiber diameter (Müller et al., 2020).

Functional connectivity relates to the temporal dependence between spatially remote neurophysiological events, which is reflected in the correlation of two spatially restricted time series in the low-frequency range (0.01-0.1 Hz) (van den Heuvel and Pol, 2010). Positive values reflect cooperation or integration and negative correlations imply segregation and antagonism between brain areas (Fornito et al., 2016). The signal time series is related to the blood oxygen level-dependent effect of increased local blood flow and volume in response to neuronal activity. Different from DTI-based structural connectivity analysis, in rs-fMRI, seed- and model-free methods co-exist. In the seed-based/atlas-based analysis, a standardized brain atlas is registered with the rs-fMRI data to derive correlations between a particular brain region against all other regions, which allows assessing the correlation between all combinations of regions (Jonckers et al., 2015; Green et al., 2018; Aswendt et al., 2021). In the model-free approach, localized resting-state patterns are extracted without a prior definition of regions using independent component analysis (ICA) to discriminate spatial sources that are maximally independent of each other (van den Heuvel and Pol, 2010). ICA is different when applied to multiple groups (disease vs. control, wild-type vs. mutant), leading to sets of components with different spatial extents and strengths (Mandino et al., 2020). Thus, comparisons at a group or study level are complex and require strategies such as multi-subject ICA combined with dual regression to facilitate statistical testing (Zerbi et al., 2015).

Despite exciting new protocols of scanning awake mice with head fixation, which best resemble human MRI conditions but require extensive training and monitoring of stress (Desai et al., 2011; Tsurugizawa et al., 2020), most protocols include anaesthetics. The selection of anaesthesia has strong influence, especially on the calculation of functional connectivity, which assumes stable physiological conditions. In the most common protocol, initial isoflurane (1-2%) anaesthesia is followed by medetomidine (MED: 0.05 mg/kg bolus, 0.1 mg/kg/h infusion) and low-dose isoflurane (ISO 0.5%) (Grandjean et al., 2014). The ISO/MED protocol takes advantage of complementary effects of both drugs related to altered hemodynamic and neurovascular coupling (e.g. vasodilation vs. vasoconstriction). Under ISO intra- and inter-cortical interactions dominate and cortico-thalamic connectivity is attenuated, whereas MED promotes subcortical connectivity including interactions between cortical and thalamic components (Bukhari et al., 2017). In a steady-state of cortical activity after the ISO to ISO/MED transition, the protocol enables reproducible functional networks in mice (Pradier et al., 2021). In addition, the ISO/MED protocol provides similar bilateral and unilateral functional networks in comparison to an awake fMRI protocol (Yoshida et al., 2016).

To remove remaining hardware and physiological noise in the data, a multi-step processing is required - especially for rs-fMRI - and typically includes motion correction, spatial smoothing, temporal demeaning, detrending and band-pass filtering, regression of nuisance covariates. As there is no consensus in the field, it can be difficult to find the best denoising approach. In a recent comparison of six nuisance regression models, the signal from ventricle and vascular masks combined with motion parameters showed best specificity of functional connectivity (Grandjean, et al., 2020). Alternatively, recordings of physiological cycles can be used as regressors, e.g. for the motion linked to the respiratory cycle (Kalthoff et al., 2011; Aswendt, Green, et al., 2021). For a more detailed overview of mouse-specific requirements, we refer to recent reviews, e.g., (Müller et al., 2020; Jonckers et al., 2015; Pan et al., 2015; Gorges et al., 2017).

The MRI-compatible mouse brain atlas

A brain atlas with a pre-defined brain structure hierarchy and coordinate system has essential advantages, as it can serve as a reference system to facilitate collaborative, comparative, and interoperable work, e.g., multi-center studies and atlas-based correlations with histology and behavior (Hawrylycz et al., 2011; Hess et al., 2018). Different from the Montreal Neurological Institute (MNI) human atlas, as one common standard brain atlas in human MRI (Mazziotta, 2002), a similar mouse MRI-compatible standard is not defined and most labs rely on a custom-made MRI template and brain atlas (Grandjean et al., 2020).

In recent atlas developments, various microscopy- or MRI-based atlases were generated (Dorr et al., 2008; Hawrylycz et al., 2011; Hess et al., 2018; Pallast, Diedenhofen, et al., 2019), which differ in image resolution and level of segmentation detail in 2D/3D (Figure 1A-B). Next to the MRI-based DSURQE atlas with 40 μm isotropic resolution and 180 defined structures, the Allen Brain Reference Atlas (ARA), represents the most detailed anatomical atlas in terms of image resolution (10 μm isotropic) and segmentation details in 3D (1327 neural structures, fiber tracts and gross anatomical details). The atlas was generated as a group average autofluorescence stack acquired from 1,675 C57BL/6J male mice using serial two-photon tomography (Oh et al., 2014). Due to differences in ontology and some anatomical delineations from the historical 2D gold standard, the atlas by Franklin and Paxinos generated from one C57BL/6J mouse (Franklin and Paxinos, 2008), there are ongoing approaches to combine and harmonize the two (Chon et al., 2019). Unique to the ARA is that in the same common coordinate framework for all regions, gene expression and viral tracing data can be retrieved (Lein et al., 2007; Oh et al., 2014) and integrated for comparison and region-wise correlations in studies of functional and structural connectivity (Mills et al., 2018; Goubran et al., 2019). To obtain an MRI-compatible ARA version split between hemispheres, we and others have proposed down-scaled versions, in which the anatomical hierarchy is maintained, and small regions that would otherwise suffer from partial volume effects were merged in larger parental regions (Pallast et al., 2019; Takata et al., 2021). Our custom version, for example, comprises 98 regions (49 per hemisphere), including important

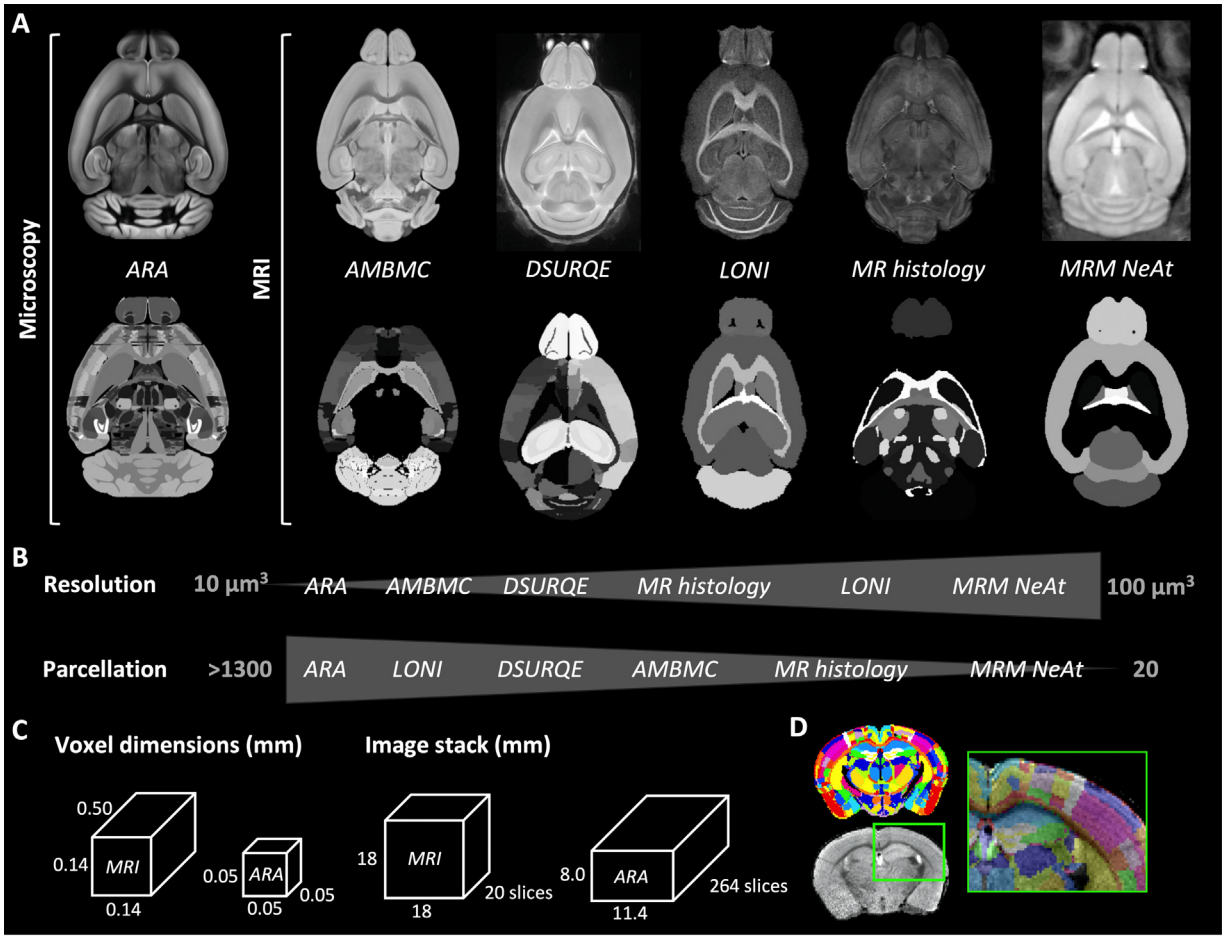

Figure 1. Digital mouse brain atlas. A) Images from currently available mouse brain atlases derived from microscopy and MRI: 1) Allen Brain Reference Atlas (ARA, (Lein et al., 2007; Wang et al., 2020)), 2) Australian Mouse Brain Mapping Consortium, AMBMC (Janke and Ullmann, 2015), 3) DSURQE (Dorr et al., 2008), 4) LONI (MacKenzie-Graham et al., 2007), 5) MR histology (Johnson et al., 2010), 6) MRM NeAt (Ma et al., 2005). Upper row shows axial section of the template and lower row the corresponding section with atlas labels. B) Illustration of differences in image resolution and parcellation. C) Differences in voxel and image stack dimensions between typical MRI - in vivo DTI (Pallast, Wieters, et al., 2020) and the ARA with 50 μm scaling. D) Example of multi-step registration result of the original ARA and a T2-weighted MRI. A and D modified from (Pallast, Diedenhofen, et al., 2019).

cortical and subcortical regions and has been successfully applied to DTI and rs-fMRI network analysis (Pallast et al., 2020; Aswendt et al., 2020; Aswendt et al., 2021). Takata et al. used a version with 100 atlas regions for rs-fMRI across the anatomical hierarchy (Takata et al., 2021). The choice of the atlas and the number and size of regions is critical for graph construction as it constraints the resolution for all following analysis and directly affects non-binary measures as a function of spatial scale (Zalesky et al., 2010).

High-quality atlas registration is essential to avoid incorrect assignment of nodes. Unlike a T2- or diffusion-weighted MRI atlas (Figure 1A), the ARA image contrast is different, e.g., the ventricles appear black, making it difficult for registration using intensity-based similarity measures. Further, voxel dimensions and size of the image stacks differ vastly between MRI and the ARA, especially in the z-component (e.g., 20 vs. 264 slices (Figure 1C). Inhomogenous shrinkage of the brain, such as in neurodegenerative diseases or acute brain lesions, requires specific optimization of registration parameters (Bachmann et al., 2018; Pallast, et al., 2019). We and others have implemented specific multi-step registration workflows (Figure 1D) using common affine and non-linear registration algorithms and software adapted from human MRI (Koch et al., 2017; Goubran et al., 2019; Pallast et al., 2019; Takata et al., 2021).

How to apply graph theory to mouse brain MRI data

Graph construction

The first step in applying graph theory is to construct a graph representing the underlying brain network. Graphs are mathematical objects defined by a set of brain areas (nodes) and their structural or functional relation (edges). Each edge represents the relation between two connected nodes and defines if the connection exists (unweighted, binary graph), the connectivity strength (weighted, undirected graph), and the order of nodes (unweighted/weighted, directed graph) (Figure 2A). Directed edges indicate a directionality of information transfer. Graphs can be stored in a square matrix of size N × N (where N is the number of nodes), the so-called adjacency matrices (Figure 2A). The number of rows and columns corresponds to the number of nodes with zeros on its diagonal. Each non-zero entry in the adjacency matrix corresponds to an edge between two nodes. In case of a weighted graph, the value of the entry quantifies the strength of the connection. Symmetric adjacency matrices correspond to undirected graphs, nonsymmetric matrices to directed graphs. For a comprehensive list of notations, see Supplementary Material Table S1.

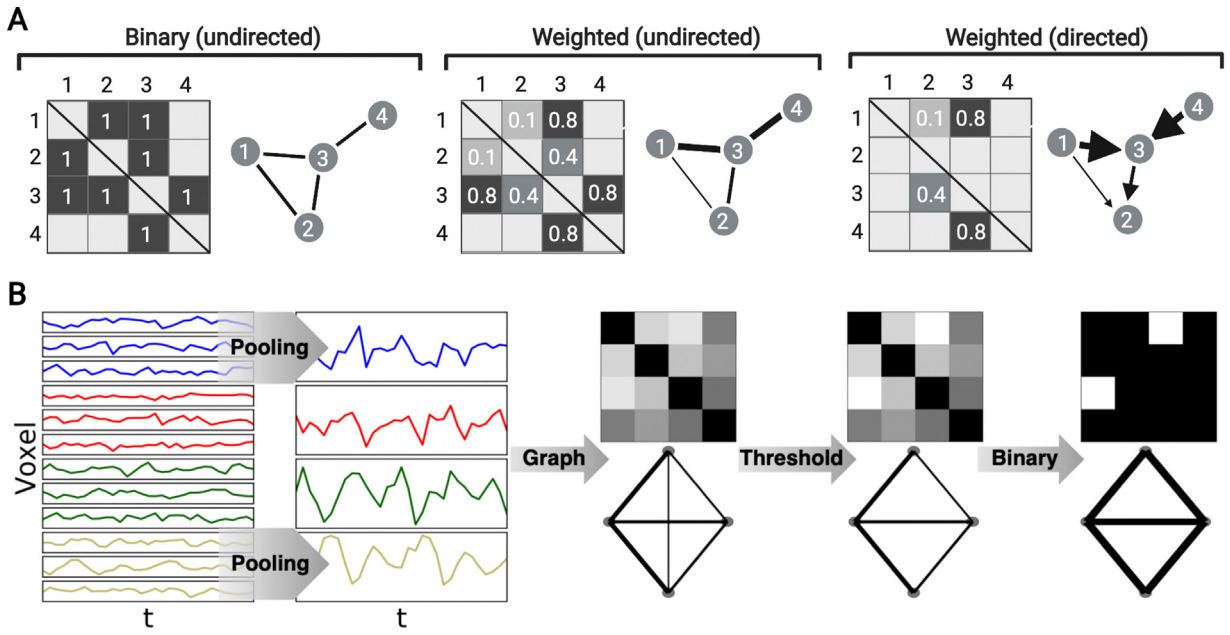

Figure 2. Graph construction and resulting adjacency matrices. A) Different types of adjacency matrices related to binarized (undirected), weighted (undirected), and weighted (directed) graphs. B) Schematic overview of typical data processing steps for graph construction in rs-fMRI including the pooling of BOLD traces in voxels related to a specific brain region. The resulting graph can be thresholded and/or binarized.

Data pooling

For rs-fMRI, the pooling relates to the (blood-oxygen-level-dependent (BOLD)) traces of single voxels to create a Region of Interest (ROI), i.e., mapping of voxels to pre-defined atlas regions by averaging across all voxels belonging to one ROI. The connectivity between the ROIs is expressed as the Pearson's correlation (for alternative models, see (Luppi and Stamatakis, 2021; Fornito, Zalesky, and Bullmore, 2016; Wang et al., 2014). The resulting graph is undirected, i.e., there is information about the functional connectivity between regions but not which region directs the activity of the other regions. Various connectivity measures exist to obtain directed graphs, e.g., Granger causality or Dynamic Causal Modelling (DCM). The resulting asymmetric matrices correspond to directed graphs of effective connectivity and include the causal influence of region A over B (Bajaj et al., 2016). These methods require a higher amount and quality of data to be reliable. The constructed graph has per definition a higher degree of freedom and the estimators have a greater complexity (Conti et al., 2019), which leads to a higher variability in the estimated links. So far, effective connectivity was successfully calculated for a small number of nodes using the Granger causality only (Karatas et al., 2021) but not for larger networks.

For DTI, the pooling and correlation operations are combined. The voxels are clustered into super-voxels that represent the ROIs. The connectivity measure counts the number of reconstructed fibers between these ROIs and constructs a symmetric matrix, as shown for the fMRI example. In both scenarios, the result is a symmetric undirected matrix representing an undirected graph, as there is no directionality of the connections included (Figure 2A). The construction of the adjacency matrices is the most important step in the application of graph theory. The resulting matrices should be checked at this stage for plausibility, e.g., for existence of wellknown connectivity patterns. All following analysis steps are an abstraction of these results. To our knowledge there is no established protocol for the quality control in pre-clinical trials.

Thresholding

Thresholding is an essential part of the analysis to filter the connectivity matrix, reduce the number of edges, and retain only connections with a high probability and minimal stochastic effects. Prior to thresholding functional connectivity data, a strategy for negative values needs to be determined. Some network measures (e.g. shortest path) require (weighted) positive networks, e.g. by setting all negative edges to 0 or taking the absolute values of all edges. Both strategies alter the "raw" connectivity and it is advisable to report in case of many negative edges a separate graph (Hallquist and Hillary, 2018). There are thresholding methods resulting in a single graph and methods which involve the analysis of a range of thresholds (Fornito, Zalesky, and E. T. Bullmore, 2016). The former includes global weight-based or density-based strategies and local strategies for network reduction, i.e., the minimum spanning-tree in which all nodes are connected with the minimal sum of edge weights (Alexander-Bloch et al., 2010). A fixed threshold to neglect connections with minor strength, i.e., to set all correlations below 0.1 to 0 and everything else to 1, is the simplest method resulting in a binarized matrix in which all connections are considered equally important (Figure 2A). Whereas such an absolute threshold shows little variability across different parcellation schemes (i.e., the number of brain regions), the resulting graphs differ in density, which can enforce/ignore nonsignificant/significant connections (Wijk et al., 2010). More stable network measures can be obtained with a proportional threshold (Garrison et al., 2015; van den Heuvel et al., 2017) by normalizing all connections to the strongest connections in each network to maintain equal network density across groups. Thus, differences in graph metrics (e.g. clustering coefficient and characteristic path length) are assumed to result from differences in the topological organization of edges and not from differences in the number of edges. As there is no lower cut-off, the inclusion of lower correlation potentially includes more random/noisy connections (van den Heuvel et al., 2017). Notably, there are opposing reports about using a fixed or proportional threshold and for many disease states no validation of an optimal threshold exists (Buchanan et al., 2020; Bachmann et al., 2018; Hallquist and Hillary, 2018). The threshold strategy should be adjusted to the experimental paradigm: if a change in density is expected to be a confounder, a proportional threshold should be chosen but if it can be interpreted as an effect of the intervention, a weight-based method might be the better solution (Fornito et al., 2016). To overcome an arbitrary distinction between important and unimportant edges, common strategies involve

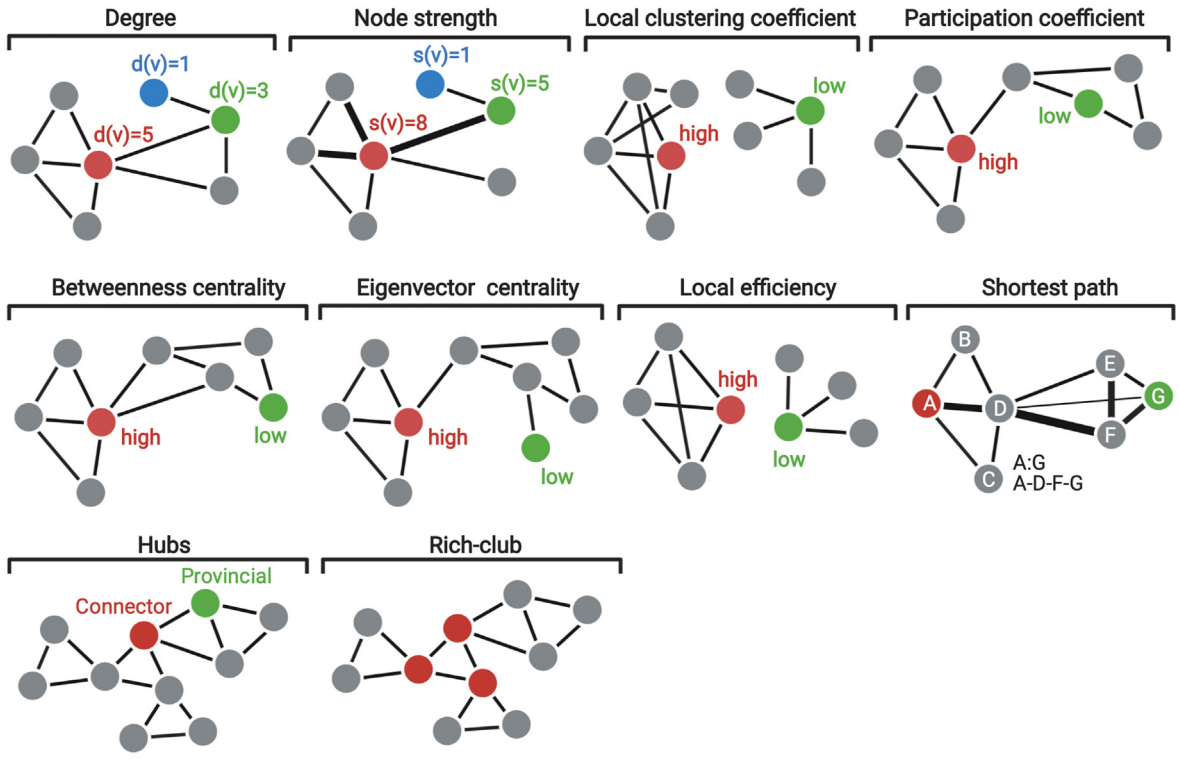

Figure 3. Illustration of local measures. Circles and connecting lines represent edges and nodes, respectively. Important nodes highlighted in red, green or blue). The route of the shortest path is shown in a weighted graph. Considering a binary graph, the shortest path then changes to A-D-G.

i) a sequence of increasing thresholds and to compare the network measures at each threshold (Fallani et al., 2014), ii) a selection (a window) of thresholds (Lohse et al., 2014), and iii) the area under the curve, in which the network measures are integrated over the full range of thresholds (He et al., 2009; Bassett et al., 2012).

Local and global network measures

This section briefly introduces the most frequently used network measures to quantify local and global changes. Notably, for some measures, e.g. the clustering coefficient, the calculation depends on the type of network (binary/weighted, directed/undirected). In our summary, we have focused on binary/weighted, undirected networks as the most common for rs-fMRI and DTI analysis. Illustrations of graphs representing local and global measures can be found in (Figs. 3 and 4).

Degree $d(v)$: $[0,|V|]$
The number of connections of a node v (neglects edge weights).

Node strength $s(v) \in \mathrm{R}$
The sum of all edge weights connected to the node v in a weighted directed or undirected graph.

Local clustering coefficient $C(v)$: $[0,1]$
The fraction of neighbors of a node that are neighbors of each other.

Participation coefficient $P(v)$: $[0,1]$
Determines if the edges of a node v tend to be clustered into one module of the network or link different specialized modules.

Betweenness centrality $b(v)$: $[0,1]$
The number of most efficient (shortest) paths in the graph that pass through the node.

Eigenvector centrality $EC(v) \in \mathrm{R}^+$
Determines if the node is connected to other nodes with high degrees.

Local efficiency $E_{loc}(v)$: $[0,1]$
Describes how well information can be transmitted in the immediate surrounding of the node v and provides a basis for effective segregated information processing in the network.

Shortest path $l_{vu:}$ $[1,n_V-1]$
The shortest path is the path between two nodes that minimizes the total edge weight along the path (sum of all involved edge weights). In a binary graph it is determined by the minimum number of edges between two nodes.

Network hubs and rich club
Network hubs are connected to a high number of nodes and/or link different subnetworks. The rich club is the tendency of connector hubs to have connections outside of their modules merely among themselves, defining a core network structure that allows efficient integration of otherwise segregated subnetworks.

Global clustering coefficient $C(G)$: $[0,1]$
The mean local clustering coefficient of all nodes in the network.

Transitivity $T(\mathrm{G})$: $[0,1]$
A variant of the global clustering coefficient, reflecting the network's tendency to be segregated into relatively independent, local neighborhoods.

Density $Den(G)$: $[0,1]$
The fraction of existing edges in the network relative to the maximal number of possible edges.

Characteristic path length $L(G) \in \mathrm{R}^+$
A measure for global connectedness, calculated as the average shortest path length between all pairs of nodes in the graph.

Global efficiency $E_{glob}(G)$: $[0,1]$
The inverse of the characteristic path length and a measure of global connectedness.

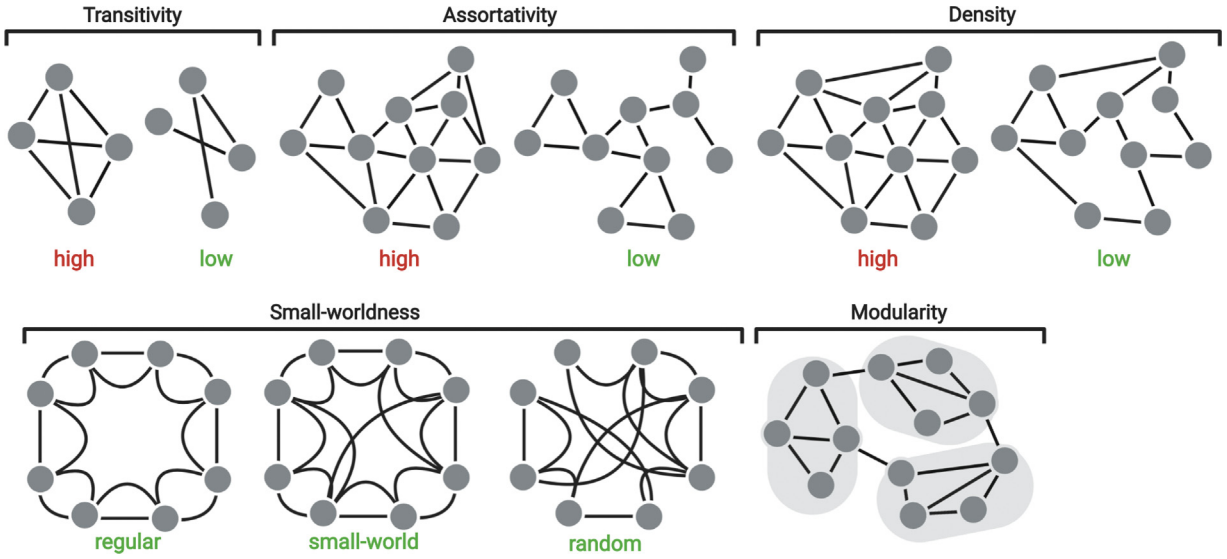

Figure 4. Illustration of global measures. Circles and connecting lines represent edges and nodes, respectively.

Assortativity $r(G)$: $[-1,1]$
Determines the tendency of networks to included nodes which connect with other similar nodes.

Modularity $Q(G)$: $[-1,1]$
Determines the degree to which the network tends to be segregated into relatively independent, non-overlapping modules (subnetworks).

Small-worldness $S(G) = \sigma(G) \in \mathrm{R}^{+}$
Networks that classify small-world properties are characterized by overall short path lengths and a high degree of clustering.

For a more detailed description about the measures, the mathematical definitions, and graphtheoretical equations, see the Supplementary Material and the BCT documentation.[1]

Processing tools

Calculating graph theoretical measures on graphs with many regions requires efficient and automated processing tools. For human brain MRI, the Brain Connectivity Toolbox (BCT) set the standard in the field of brain network analysis (Rubinov and Sporns, 2010). As the BCT is a library of functions that work with adjacency matrices, it is also suitable for mouse brain MRI and other species. However, for many functions it is worth embedding them in larger, in-house developed scripts, for example to compare multiple groups or to display the results in a plot. Furthermore they can help to simplify the usage of the functions. However, in order for results to remain comparable, it is beneficial to establish common software pipelines. In addition to existing toolboxes, which include only a selection of network algorithms and/or an adaption to human MRI (e.g., MagnAn and CONN), we provide with AIDAconnect the first atlas-based toolkit dedicated to mouse brain MRI and a comprehensive collection of BCT-based ready-touse scripts (https://github.com/aswendtlab/AIDAconnect). AIDAconnect is a wrapper for the BCT functions, it covers scripts to calculate local and global measures, e.g., the degree of a region at multiple time points or the shortest path between two regions. AIDAconnect requires a matrix containing the time series per brain region or the number of fiber tracts between brain regions as input. For convenience, AIDAconnect is tailored to our preprocessing pipeline AIDAmri (Pallast et al., 2019), which provides this input shape. To visualize network measures, automated plot functions are included, e.g. for local and global measures over time for multiple groups. We have also included additional scripts that go beyond the functionality of the BCT, for example to calculate new or lost connections between two time points, to calculate the n-strongest connections of a region and scripts to display the degree or strength distribution. Further scripts plot the alteration of certain edge weights over time or display the connectivity of pre-selected subgraphs in anatomically correct 2D grids. The combination of functions allows more advanced calculations, e.g. to classify certain regions as network connector hubs. As hub nodes usually are determined by a high degree value, the included degree distribution function lists all regions in a certain degree range, which is used to determine the ones with the highest degree. Connector hubs are further characterized by having connections to other nodes or modules (van den Heuvel and Sporns, 2013). Thus, local measures that describe centrality are applied for these high-degree regions in a next step, e.g. the participation coefficient, which tends to be close to 1 if the node's edges are uniformly distributed among all existing modules (Guimerà and Amaral, 2005). This way, AIDAconnect was already successfully applied to longitudinal DTI and rs-fMRI data in experimental stroke studies (Pallast et al., 2020; Aswendt et al., 2020; Aswendt et al., 2021).

Statistical tests

Statistical tests for networks between multiple groups require similar care as time series/fiber tracking data, which have been discussed in detail elsewhere (Kim et al., 2014). For both local and global measures, the typical statistical pitfalls apply: the statistical group comparisons based on individual connections require a correction for multiple testing, e.g, based on the false discovery rate (FDR), which reduces statistical power drastically when applied on large networks. Comparisons on a network level is simpler, however, lacks specificity and power to determine changes in only a small subset of the whole neural network (Fornito et al., 2016). The same hypotheses have to be tested many times to localize effects to single nodes or even single edges. This leads to the multiple comparison problem and needs to be corrected. The widely used Bonferonni-, Šidák- and Holm-Bonferonni corrections are highly conservative and may obscure true positives. These methods provide strong control of familywise errors. The family consists of all nodes or edges tested. The robust control ensures that a rejection of the null-hypotheses is valid (Fornito et al., 2016). Weak control of family-wise errors can increase the statistical power. An example is the false discovery rate (Benjamini and Hochberg, 1995), which ensures a maximum rate of falsely rejected null hypotheses. For cases with no rejected null

[1] https://sites.google.com/site/bctnet/list-of-measures

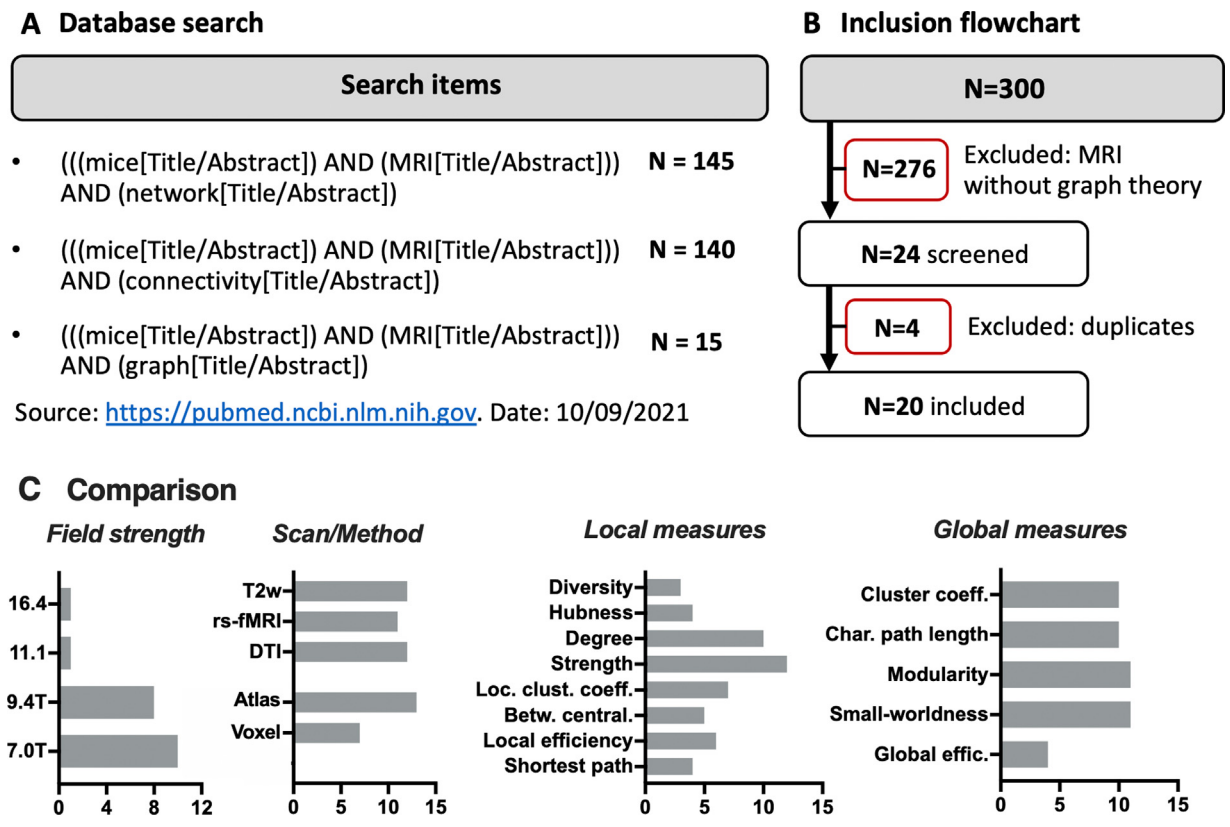

Figure 5. Selection of MR neuroimaging studies using graph theory in mice. A) Selection diagram showing the number of studies from the database search. B) Quantitative comparison of mouse brain MRI studies using graph theory based on the field strength, scan, method for graph construction, and how often local and global measures were applied. Note: all measures that occurred only once were excluded and the measures 'Hubness', 'Hub Scores' and 'Hub Tendency' were summarized as 'Hubness'.

hypothesis, weak and strong control yield the same result. A rejected null hypothesis leads to an overall rejection because the weak control of family-wise errors discriminates between individual hypotheses. The listed corrections do not consider the spatial and topological features inherent to brain networks. Methods considering these features can increase the statistical power. These class methods are, for example, the network-based statistic (Zalesky et al., 2011), which provide a weak control of the familywise error.

Most animal neuroimaging studies are underpowered with sample sizes below 10 per group (Mandino et al., 2020). Small sample sizes yield a poor fit of the parametric test distributions like the Student's t-distribution. The construction of an empirical test distribution by permutation tests can be beneficial for the small group sizes. These tests use the collected data set and permute the group assignments in each sample to construct the test distribution. This class accounts for dependencies between tests inherently present in brain networks due to their spatial and topological structure but can also be introduced by the method to construct the graph (Fornito et al., 2016; Good, 1994).

MRI network studies in mice

We searched PubMed for articles related to the keywords in the title/abstract: "graph theory, network, connectivity" + "mice" + "MRI" and collected 300 studies. From that initial list, unrelated studies and duplicate findings were excluded. Finally, 18 studies were included (Figure 5A). The rat stroke study by van Meer et al. was also included because it was one of the first experimental studies of brain disease to use graph theory and serves as a (historical) reference here. In Table 1 the disease model, MRI protocol, image processing, graph-based measures, availability of code/data, the applied software tools for graph theory, and the statistics are summarized. Most studies were conducted at 7.0T and 9.4T using high-resolution T2-weighted MRI as reference, and rs-fMRI and DTI protocols at similar frequency. More studies applied an atlas-based analysis. The basic local measures degree and strength were most frequently used. Other local measures, e.g., local efficiency and betweenness centrality were much less applied. The global measures modularity, clustering coefficient, characteristic path length, and small-worldness were applied most. In contrast, global efficiency was used less often. Other commonly used measures in graph theory that describe centrality features of a node, e.g., closeness centrality, eigenvector centrality, or participation coefficient, were not part of the discussion in these studies. The processing tools and mathematical definitions used to construct the graphs and calculate the network measures could not be compared as most either the code and or the raw data were not available for re-evaluation. In this line, there was no consensus on the statistical tests.

Interpretations

The interpretation of graph theoretical measures is difficult to standardize and depends on how the MRI data were collected or which disease model was studied. The animal models reviewed here, differ substantially, and, therefore, we could not extract a general interpretation for network measures. While in human MRI, a decrease in global efficiency is a validated biomarker for detecting dementia in patients with small vessel disease and age-related mild cognitive impairment (Lawrence et al., 2014; Berlot et al., 2016), biomarkers remain to be established for pre-clinical studies. Based on the selected studies, we provide an overview of previous attempts to describe the underlying biological processes that contribute to graph network alterations. The interpretation is structured in three categories of network measures:

Table 1
Overview of mouse brain studies (in alphabetical - first author - order)

Study	(Aswendt, Green, et al., 2021)
MRI Protocol	9.4T: T2w: 0.068 × 0.068 × 0.3 mm, rs-fMRI (EPI): 0.182 × 0.182 × 0.4 mm
Atlas- / voxel-based	Atlas-based (custom Allen Reference Atlas CCF v3 (Lein et al., 2007), 49 regions per hemisphere)
Graph-based measures	**Local:** *d,s* **Global:** *C,Den,L,Q*
Code / Data available	Yes[1] / Yes[2]
Tools	AIDAmri (Pallast, Diedenhofen, et al., 2019) and AIDAconnect
Statistics	Two-way ANOVA with false discovery rate (FDR) correction for group comparisons
Disease model	Stroke (photothrombosis model)
Study	(Barbeito-Andrés et al., 2018)
MRI Protocol	9.4T: T2w: 0.117 × 0.117 x NA mm, DTI: NA
Atlas- / voxel-based	Atlas-based (Allen Reference Atlas (Lein et al., 2007), 24 ROIs)
Graph-based measures	**Local:** *b,C,d,*E_{loc} **Global:** *C,L,S,median weight value,rich club coefficient*
Code / Data available	No / No
Tools	Custom tools based on the Brain Connectivity Toolbox (Rubinov and Sporns, 2010), igraph[3] in R
Statistics	Bartlett-Test to assess similarity of variances between groups
Disease model	Effect of maternal nutritional restriction during pregnancy on offspring brain development
Study	(Blaschke et al., 2021)
MRI Protocol	9.4T: T2w, rs-fMRI (EPI) 0.182 × 0.182 × 0.5 mm
Atlas- / voxel-based	Atlas-based (custom Allen Reference Atlas CCF v3, 49 regions per hemisphere)
Graph-based measures	**Local:** *s* **Global:** *L,S,mean node strengh s*
Code / Data available	No / No
Tools	AIDAmri (Pallast, Diedenhofen, et al., 2019) and custom Matlab tools based on the Brain Connectivity Toolbox (Rubinov and Sporns, 2010)
Statistics	Group differences in global network parameters between stroke and individual controls tested by either independent t-Test or Mann-Whitney-U-Test with post-hoc FDR correction
Disease model	Stroke (photothrombosis and dMCAO model)
Study	(Boehm-Sturm et al., 2017)
MRI Protocol	7T: T2w: 0.1 × 0.1 × 0.45 mm, DTI: 0.225 × 0.225 × 0.225 mm
Atlas- / voxel-based	Atlas-based (atlas not specified, 7 ROIs)
Graph-based measures	**Local:** *d,*E_{loc} **Global:** *C,*E_{glob}*,Q,T*
Code / Data available	No / No
Tools	Not specified
Statistics	Paired t-test (time comparison), Mann–Whitney-U-test (clustering coefficient) and unpaired t-test for group comparison
Disease model	Brain hypoperfusion
Study	(Cerina et al., 2020)
MRI Protocol	9.4T: T2w: NA, DTI (EPI): 0.125 × 0.125 × 0.3 mm
Atlas- / voxel-based	Atlas-based (Allen Reference Atlas CCF v3 (Lein et al., 2007), 82 ROIs)
Graph-based measures	**Local:** *None* **Global:** *C,Q*
Code / Data available	No / Yes[4]
Tools	Custom tools based on the Brain Connectivity Toolbox (Rubinov and Sporns, 2010)
Statistics	One-way ANOVA for group and time point comparison incl. post-hoc Tukey's or Bonferroni's tests
Disease model	Demyelination (Cuprizone treatment)
Study	(Colon-Perez et al., 2019)
MRI Protocol	11.1T: T2w (RARE): 0.059 × 0.043 × 0.7 mm, rs-fMRI (EPI): 0.234 × 0.229 × 0.9 mm, DTI (EPI): 0.117 × 0.117 × 0.7 mm
Atlas- / voxel-based	Atlas-based (Multi-Atlas Label Fusion (Ma et al., 2014), 90 ROIs, 45 per hemisphere) with additional ICA (20 predetermined components) and PCA (projection into 12, 20 and 30-dimensional subspace)
Graph-based measures	**Local:** *C* **Global:** *L,Q,S,global node strength*
Code / Data available	No / No
Tools	Custom tools based on the Brain Connectivity Toolbox (Rubinov and Sporns, 2010)
Statistics	Two-factor ANOVA (Strain x Treatment) and Tukey's post-hoc test
Disease model	Amyloidosis (Quantifying microstructural changes for potential biomarkers using neurite orientation dispersion and density imaging)
Study	(Fernández-García et al., 2020)
MRI Protocol	7.0T: T2w (RARE): 0.08 × 0.08 × 0.5 mm, rs-fMRI (EPI): 0.21 × 0.21 × 0.5 mm
Atlas- / voxel-based	Atlas-based using the Magnetic Resonance Microscopy Atlas (20 ROIs) (Ma et al., 2008)
Graph-based measures	**Local:** E_{loc}*,s* **Global:** *C,*E_{glob}
Code / Data available	No / No
Tools	Custom (not specified) based on the Brain Connectivity Toolbox (Rubinov and Sporns, 2010)
Statistics	Two-tailed Student's t-test or Two-way ANOVA incl. post-hoc Bonferroni's tests
Disease model	Huntington mouse model
Study	(Grandjean, Zerbi, et al., 2017)
MRI Protocol	9.4T: rs-fMRI (ME-EPI): 0.3 × 0.3 × 0.3 mm
Atlas- / voxel-based	Voxel-based (group-ICA with 30 pre-determined components, 17 components with plausible anatomical locations)
Graph-based measures	**Local:** *l* **Global:** *None*
Code / Data available	No / Yes[5]
Tools	igraph[3] in R
Statistics	Two-way t-test for correlation comparison
Disease model	No disease model (Comparison of functional connectivity with the underlying monosynaptic structural connectome as provided by the Allen Mouse Brain Connectivity Atlas)

(*continued on next page*)

Table 1 (*continued*)

Study	(Hübner et al., 2017)
MRI Protocol	7T: T2w: 0.051 × 0.051 × 0.3 mm, rs-fMRI (EPI): 0.15 × 0.15 × 0.7 mm, DTI (DT-EPI): 0.094 × 0.094 × 0.5 mm
Atlas- / voxel-based	Voxel-based (group ICA tested with ICASSO ((Himberg et al., 2004), 90 components) with a following overlap identification using the Allen Reference Atlas (Lein et al., 2007) resulting in 82 ROIs
Graph-based measures	**Local:** *s* **Global:** *C,L,Q,S*
Code / Data available	No / No
Tools	Not specified for the calculation of graph measures
Statistics	two-sample t-test for group comparison, heterogeneous variances and FDR corrected
Disease model	Demyelination (Comparative evaluation of structural vs. functional connectivity after Cuprizone treatment)
Study	(Iturria-Medina et al., 2013)
MRI Protocol	7T: DTI: 0.08 × 0.08 × 0.08 mm
Atlas- / voxel-based	Atlas-based (Waxholm Space mouse brain atlas (Johnson et al., 2010), 26 gray matter regions parcellated into 75 ROIs per hemisphere)
Graph-based measures	**Local:** E_{loc} **Global:** C,E_{glob},L,S
Code / Data available	No / Yes[6]
Tools	Not specified
Statistics	Correlation coefficients for subject comparison
Disease model	No disease model (General estimation of graph measures)
Study	(Karatas et al., 2021)
MRI Protocol	7T: T2w: 0.051 × 0.051 × 0.3 mm, rs-fMRI (GE-EPI): 0.15 × 0.15 × 0.7 mm, DTI (DT-EPI): 0.094 × 0.094 × 0.5 mm
Atlas- / voxel-based	Atlas-based (Allen Reference Atlas (Lein et al., 2007), 37 ROIs)
Graph-based measures	**Local:** *Hubness,s,Stouffer coefficients* (Stouffer, 1936) **Global:** *None*
Code / Data available	No / No
Tools	In-house developed MATLAB Tools
Statistics	One-sample t-test to identify statistically significant edges, FDR corrected and two-sample t-test for group differences
Disease model	No disease model (Comparison of structural and functional connectivity between C57BL/6 and BALB/cJ mice)
Study	(Komaki et al., 2016)
MRI Protocol	7T: T2w (RARE): 0.051 × 0.051 × 0.3 mm, DTI (EPI): 0.094 × 0.094 × 0.5 mm
Atlas- / voxel-based	Voxel-based (576 subdivisions based on Allen Brain Reference atlas)
Graph-based measures	**Local:** *b,C,d,*E_{loc}*,EC* **Global:** *None*
Code / Data available	No / No
Tools	CONN (Whitfield-Gabrieli and Nieto-Castanon, 2012), Brain Connectivity Toolbox (Rubinov and Sporns, 2010)
Statistics	Paired t-test (graph measures) and FWE-corrected two-sample t-test (functional connectivity) for group comparison
Disease model	Peripheral nerve injury (neuropathic allodynia)
Study	(Kreitz et al., 2020)
MRI Protocol	9.4T: rs-fMRI (EPI): 0.117 × 0.117 × 0.5 mm
Atlas- / voxel-based	Both Atlas-based (in-house digital 3D brain atlas, 211 ROIs according to (Franklin and Paxinos, 2008)) and Voxel-based (ICA with Multi Seed Region Approach)
Graph-based measures	**Local:** *C,d,local L,s,Hub Scores HITS* (Kleinberg, 1999) **Global:** *C,L,S,customized Q* (Blondel et al., 2008)
Code / Data available	No / No
Tools	Custom, Network Workbench Tool[7], Network based statistics (NBS, (Zalesky et al., 2010))
Statistics	Two-factor ANOVA withinteraction for group comparison incl. post-hoc Tukey's test, homoscedastic two sided t-test for significant differences per brain structure incl. FDR correction
Disease model	Impact of maternal immune activation (MIA, treatment of pregnant mice with Poly(I:C)) on the brain of the adult offspring
Study	(Liu et al., 2016)
MRI Protocol	16.4T: Diffusion-weighted (SE): 0.1 × 0.1 × 0.1 mm
Atlas- / voxel-based	Atlas-based: CAI (Centre for Advanced Imaging, University of Queensland) and JHU MRI atlas (Johns Hopkins University).
Graph-based measures	**Local:** *b,d* **Global:** *S,Q*
Code / Data available	No / No
Tools	GRETNA[8] (Wang et al., 2015)
Statistics	NBS (Zalesky et al., 2010)
Disease model	Adolescent socially isolated mice
Study	(Liska et al., 2015)
MRI Protocol	7T: T2w (RARE): 0.1 × 0.1 × 0.5 mm, rs-fMRI (EPI): 0.2 × 0.2 × 0.5 mm
Atlas- / voxel-based	Voxel-based: 16,135 × 16,135 connectivity matrix was calculated for each subject using Pearson product–moment correlation coefficient.
Graph-based measures	**Local:** *s, within module s,Diversity* **Global:** *customized Q* (Blondel et al., 2008)
Code / Data available	No / No
Tools	NA
Statistics	subject-wise connectivity matrices were partitioned and the similarity of each pair of individual partitions was quantified with the variation of information (VI) metric (Rubinov and Sporns, 2010)
Disease model	No disease model (Mapping of functional connectivity hubs at voxelscale)
Study	(Mechling, Hübner, et al., 2014)
MRI Protocol	7T: rs-fMRI (EPI): 0.15 × 0.15 × 0.7 mm
Atlas- / voxel-based	Voxel-based (Group ICA to form averaged functional clusters using ICASSO (Himberg et al., 2004), 92 components)
Graph-based measures	**Local:** *d,Diversity,Hub Tendency,s* **Global:** *C,L,Q,S*
Code / Data available	No / No
Tools	Graph theory methods as described by (Newman, 2006)
Statistics	Not specified for graph measures, one-sample t-test for statistical relevance of direct connectivity
Disease model	No disease model (Large-scale mouse brain functional connectivity (MBFC))

(*continued on next page*)

Table 1 (*continued*)

Study	(Mechling, Arefin, et al., 2016)
MRI Protocol	7T: T2 (RARE): 0.051 × 0.051 × 0.3 mm, rs-fMRI (EPI): 0.15 × 0.15 × 0.75 mm, DTI (EPI): 0.094 × 0.094 × 0.5 mm
Atlas- / voxel-based	Voxel-based: Identification of clusters as nodes via ICA (100 components), followed by registration with the Allen Reference Atlas to select 87 functional clusters
Graph-based measures	**Local:** *C,Diversity,s* **Global:** *L,Q,S*
Code / Data available	Yes[9] / No
Tools	Graph theory methods as described by (Newman, 2006)
Statistics	ICASSO to assess pattern stability, no statistical group comparison
Disease model	Mu opioide rececptor knockout mice (Oprm1-/-) vs control mice
Study	(Meningher et al., 2020)
MRI Protocol	7T: DTI (EPI): 0.21 × 0.21 × 0.21 mm
Atlas- / voxel-based	Atlas-based (DSURQE atlas[10], 68 ROIs) Voxel-based analysis for structural alteration analysis in gray matter brain regions
Graph-based measures	**Local:** b,Cl,d,E_{loc},s **Global:** E_{glob}
Code / Data available	No / No
Tools	Network Analysis Tool embedded in ExploreDTI[11], Brain Connectivity Toolbox (Rubinov and Sporns, 2010) in combination with custom MATLAB scripts
Statistics	Mixed design ANOVA with group and time point effect, FDR corrected
Disease model	Mild traumatic brain injury (mTBI)
Study	(Pallast, Wieters, et al., 2020)
MRI Protocol	9.4T: T2w: 0.068 × 0.068 × 0.4 mm, DTI (EPI): 0.14 × 0.14 × 0.5 mm
Atlas- / voxel-based	Atlas-based (custom Allen Reference Atlas CCF v3 (Lein et al., 2007), 49 regions per hemisphere, 13 per hemisphere selected for graph analysis)
Graph-based measures	**Local:** *d,l,s* **Global:** *None*
Code / Data available	Yes[12] / Yes[13]
Tools	Brain Connectivity Toolbox (Rubinov and Sporns, 2010)
Statistics	Mixed-effects analysis (Greenhouse-Geisser correction) for time point and group comparison, post-hoc multiple comparisons FDR corrected
Disease model	Stroke (photothrombosis model)
Study	(Pradier et al., 2021)
MRI Protocol	9.4 T: rs-fMRI (EPI): 0.35 × 0.325 × 0.5 mm
Atlas- / voxel-based	Atlas-based (custom mouse brain atlas with 188 ROIs derived from the Franklin and Paxinos mouse brain atlas (Franklin and Paxinos, 2008))
Graph-based measures	**Local:** *authority,b,C,d,hubscore,average l,s* **Global:** *C,L,S,customized Q* (Blondel et al., 2008)
Code / Data available	No / No
Tools	MagnAn[14]
Statistics	Network based statistics NBS (Zalesky et al., 2010) as implemented in MagnAn
Disease model	No disease model (Influence of medetomidine/isoflurane anaesthesia)
Study	(van Meer et al., 2012)
MRI Protocol	4.7T: T2w, DTI (EPI), rs-fMRI (EPI): 0.5 × 0.5 × 1.5 mm
Atlas- / voxel-based	Voxel-based (Probabilistic ICA to extract a group-averaged functional network, 7 components)
Graph-based measures	**Local:** *C,l* **Global:** *S*
Code / Data available	No / No
Tools	Custom (not specified), C++ Boost Graph Library[15]
Statistics	Two-sample paired t-tests (time point comparison), Mann–Whitney-U-test (sensorimotor performance scores), Repeated-measures linear mixed model (network parameters over time and between groups) with post-hoc Tukey's test
Disease model	**Rat**: Stroke (MCAO model)

[1] https://edmond.mpdl.mpg.de/imeji/collection/Ce5QnWU4SktzEPN
[2] https://github.com/aswendtlab/Project_Microbiome
[3] https://igraph.org/r/
[4] https://www.dropbox.com/sh/xmxmzosxrudpx1l/AABM7L_jtkd2z6oi3pnqVNZoa?dl=0
[5] http://doi.org/10.5905/ethz-1007-59
[6] https://www.nitrc.org/projects/birn/
[7] http://nwb.slis.indiana.edu
[8] https://www.nitrc.org/projects/gretna/
[9] https://www.uniklinik-freiburg.de/mr-en/research-groups/diffperf/fibertools.html
[10] https://github.com/CoBrALab/documentation/wiki/DSURQE-atlas-hierarchical-downsample
[11] https://www.exploredti.com
[12] https://github.com/aswendtlab/AIDAconnect
[13] https://doi.gin.g-node.org/10.12751/g-node.okz5nn
[14] http://www.biocom-online.de/products_ip.html
[15] https://www.boost.org/doc/libs/1_66_0/libs/graph/doc/index.html

1 connectivity strength: relates to the edge weights, which are either based on the correlations (rs-fMRI) or fiber counts (DTI)
2 network segregation: describes the tendency of the brain to divide itself into relatively independent, specialized subunits
3 network efficiency: describes how well the subunits are interconnected (integrated) to allow effective segregated information processing (Rubinov and Sporns, 2010; Farahani et al., 2019).

Connectivity strength

Connectivity strength is the most fundamental parameter calculated as edge weight, influencing node strength and various other network measures. In a longitudinal structural connectivity study of experimental stroke, we previously described specific de- and increased connectivity strength, e.g., in ipsilesional cortico-cortical and interhemispheric thalamo-cortical fiber tracts, respectively, which correlated with sensorimotor behavior (Pallast et al., 2020). Kreitz et al. observed alterations in functional connectivity and anatomical size of different brain regions in a model of maternal immune activation on the brain of adult offspring by the treatment of pregnant mice. A significantly smaller size of the corpus callosum and a reduced connectivity strength were suggested to be related to impaired functional connectivity between both hemispheres. However, no changes in global graph measures and hub functionality were observed, indicating that the overall efficiency of information integration remained the same (Kreitz et al., 2020). In the cuprizone model, inducing oligodendrocyte death and demyelination, Hübner et al. observed decreased strength values in default mode network (DMN) nodes (Hübner et al., 2017). These studies are in line with the common interpretation of structural and functional connectivity to be directly related to axonal connectivity and functional communication.

Network segregation

Clustering coefficient

Several acute injury studies reported an increased clustering coefficient as part of a compensatory effect inside and around the affected area, i.e., neuronal loss or disturbed signal synchronization followed by reduced signal correlations and functional connectivity (van Meer et al., 2012; Cerina et al., 2020; Boehm-Sturm et al., 2017; Komaki et al., 2016; Meningher et al., 2020; Blaschke et al., 2021). Further, an increased clustering coefficient was linked to demyelination in a multiple sclerosis mouse model and interpreted as a cost-efficient cerebral reorganization with strengthened local information flow (Cerina et al., 2020). Increased local connectivity of neighbors could be related to mechanisms of neural plasticity, initial recruitment, and unmasking of diffuse redundant neuronal pathways, and a reset of synaptic activity. Consequently, there could be an increase in random integration between neurons resulting in overconnectivity (van Meer et al., 2012). In an experimental stroke study, van Meer et al. reported that the clustering coefficient undergoes a dynamic change: the initial increase is followed by a decrease, which has been interpreted as part of the normalization process during post-stroke recovery, which involves the decline of redundant neuronal connections (van Meer et al., 2012). Notably, the dynamic change depended on the stroke lesion size, i.e., the clustering coefficient in large strokes did not reach the baseline level, which likely reflects a more extensive and widespread recruitment during the recovery process, e.g., of contralesional homologous cortical tissue, and significant rewiring of corticospinal tracts (Jones and Adkins, 2015). In contrast, Mengingher et al. reported a different clustering coefficient dynamic for mild traumatic brain injury in a subset of analyzed regions. Here, the local clustering coefficient decreased until 7 days with a subsequent increase at 30 days post injury (Meningher et al., 2020). The authors suggested that the initial decrease is related to diffuse axonal injury, followed by network reorganization, including axonal sprouting, to create new local connections and overcome the structural loss.

Local efficiency

Local efficiency is based on the connectivity of the local neighborhood. Thus, the interpretation is also related to similar neural plasticity mechanisms. An increase in local efficiency in mouse models of small vessel disease and neuropathic pain (Boehm-Sturm et al., 2017; Komaki et al., 2016), was suggested a compensatory effect, in which local areas increase their connections due to a decline in the connectivity between larger functional subnetworks.

Transitivity and modularity

In addition to an increase in the clustering coefficient and local efficiency, an increased transitivity and a decreased modularity were reported only by two studies. In the small vessel disease model, Boehm-Sturm et al. base their interpretation on changes in tissue microstructure within particular network hubs and a reduced number of heavily interconnected subgroups leading to less distinct subnetworks in response to hypoperfusion. They further proposed that a compensatory effect occurs due to an overall decline in the connectivity between more extended functional subnetworks. Consequently, closely connected structures might increase their connections. In another study Modularity derived from DTI connectome negatively correlated with locomotor activities and positively correlated with contextual fear conditioning and tone fear conditioning (Blaschke et al., 2021). The authors report a decreased Modularity of social isolated mice and suggest not fully matured brain circuits as explanation. The absence of social experience may disrupt axonal pruning of neuronal pathways including the orbitofrontal cortex. A decreased Modularity was also found in germ-free mice compared to control mice with healthy gut microbiom. Interestingly, in germ-free mice the pyramidal spine density was positively correlated with the global network density suggesting that the global network is denser but less structural organized (Aswendt et al., 2021). In contrast, an increase of modularity over 5 weeks was reported for the cuprizone model of widespread demyelination in mice. Cerina et al. suggested that brain network modifications during the remyelination phase occurred concerning long-range structural similarity and led to more local homogeneity (Cerina et al., 2020).

Network efficiency

Shortest path

In a previous experimental stroke study, we observed improved shortest paths between ipsilesional striatum and contralesional motor cortex, which we suggest relates to compensatory relearning of motor tasks after stroke and thus a change in network efficiency (Pallast et al., 2020). Van Meer et al. observed a deteriorated shortest path after stroke in the bilateral sensorimotor cortices, expressed by an increased shortest path length (van Meer et al., 2012). The authors suggested an increasing random integration between neurons due to the stroke lesion, following a state of overconnectivity and hyperexcitability. A subsequent decline of the shortest path length back to baseline level during post-stroke recovery was linked to dendritic pruning and synaptogenesis, leading to the abolishment of nonessential connections (van Meer et al., 2012). However, different from our cortical stroke study (Pallast et al., 2020), van Meer et al. observed a persistently increased shortest path length in large cortico-striatal strokes potentially related to the recruitment of contralesional homologous cortical tissue and significant rewiring of the corticospinal tracts (Jones and Adkins, 2015).

Small-worldness

Small-worldness was proposed as a crucial aspect of efficient brain organization as changes correlate with brain disease states. It should be noted that analysis steps, e.g., the parcellation detail and graph density, strongly interfere with the calculation and complicate the interpretation between studies (Hilgetag and Goulas, 2015). Huebner et al. found preserved small-worldness values after demyelination processes, suggesting a compensatory mechanism to maintain network efficiency

(Hübner et al., 2017). Likewise, Kreitz et al., who also hypothesized demyelination, could not observe any changes in global measures like small-worldness, indicating that the overall network efficiency was unaffected (Kreitz et al., 2020). In the small cortical stroke models (PT and dMCAO) in mice small-worldness was found to be increased at day 3 and to negatively correlate with recovery (Blaschke et al., 2021). In the large stroke model (MCAO) in rats, small-worldness was found to be increased subacutely (until 2 weeks post stroke), followed by a decrease towards baseline levels. The dynamic change might reflect the initial overshoot in neuronal clustering and wiring in response to the localized network disturbance induced by the stroke, which stabilized for efficient processing in a later phase (van Meer et al., 2012).

Mouse-specific studies combining structural and functional connectome data

Graph theory applied to the structural and functional mouse brain connectome provides the unique opportunity to uncover common organizational principles underlying neural processing. Experimental studies in mice benefit from tools to specifically manipulate brain activity, e.g. using opto- and chemogenetics, in combination with MRI (Desai et al., 2011; Ryali et al., 2016; Peeters et al., 2020), and a rich portfolio of open access databases, which in contrast to humanspecific databases, extend to gene expression, electrophysiological properties, and viral tracing (Lein et al., 2007; Oh et al., 2014; Wang et al., 2020.).

The viral tracing data defines the current gold standard to generate weighted graphs with known start and endpoints, which are defined by the tracer injection site and the loss of fluorescence signal. Conversely, it is possible to validate whole-brain in vivo and ex vivo tractography. While the 3D colocalization of reconstructed fiber tracts might differ between both data sets, the overall correlation between larger brain structures is high (Calabrese et al., 2015; Goubran et al., 2019), which makes DTI the method of choice for studies of white matter reorganization (Pallast et al., 2020). In our studies (Pallast et al., 2020; Aswendt et al., 2020), we found strong positive correlations when comparing in vivo DTI fiber tracts with the fluorescence projection volume derived from the Allen Mouse Brain Connectivity Atlas (Oh et al., 2014) for pre-selected regions. In comparing of in vivo rs-fMRI functional connectivity with post mortem DTI and viral tracing of the rat brain, positive correlations were found between rs-fMRI and DTI connectomes but not for rs-fMRI and viral tracing (Straathof et al., 2020). This study highlights that a robust functional connection between homotopic cortical areas does not implicate a solid structural connection, despite the presence of the corpus callosum. The correlation between rs-fMRI and viral tracing mouse data is different when BOLD signal dynamics are considered (Oh et al., 2014). When comparing 184 atlas regions from the Allen Mouse Brain Connectivity Atlas, strong correlations were found for the degree and clustering coefficient, among other network properties derived from weighted connectomes (Sethi et al., 2016). The combination of in vivo and ex vivo connectomes is particularly helpful for identifying structural-functional relations. Using individual DTI-based network models for simulations of functional connectivity with The Virtual Brain (TVB), it was possible to show that individual structural connectivity predicts individual functional connectivity better than an averaged structural connectivity brain, and predictions can be improved by considering fiber directionality, coupling weights and specific fiber tracts derived from the Allen connectivity atlas (Melozzi et al., 2019). In addition to individual variability, the genetic background of mouse strains imposes inter-strain differences in functional and structural networks as shown, e.g., for C57BL/6 and BALB/c mice (Karatas et al., 2021). In a voxel-based approach not pre-restricting the analysis using a parcellated connectome, a directed graph was calculated from a novel voxellevel data-driven model of the Allen Mouse Brain Connectivity Atlas (Knox et al., 2019). The analysis adds to the previous finding of evolutionarily-conserved, mutually-interconnected functional hubs in the mouse brain (Liska et al., 2015) and revealed segregated source and sink hubs embedded in a global hierarchy. Higher-order cortical areas serve as primary sources of neural input, and subcortical relay stations act as important intermodular connector hubs. The removal of global hubs was not related to a breakdown of network integrity and efficiency compared to a random node deletion (Coletta et al., 2020). These results suggest that the voxel-level mouse connectome is highly resilient to targeted removal of hub regions, initially defined as critical for network integrity and stability.

Despite the similarities in global network organization, the differential vulnerability of the human vs. mouse networks against targeted attacks warrants further studies comparing functional vs. structural networks at different levels of resolution. A better understanding of such differences will be essential for future translational studies using voxel-based vs. atlas-based parcellation of connectome data. In a recent translational atlas-based comparison, Blaschke et al. found the network parameters small worldness, characteristic path length and clustering coefficient to follow a similar pattern in the postacute stroke phase in patients compared to two cortical stroke models in mice (Blaschke et al., 2021).

Practical steps for greater use of graph theory in mouse neuroimaging

Translational studies in mouse models of neurological disorders currently lack behind the use of graph theory in human studies. As shown, only a few mouse brain MRI studies exist focusing on network measures to *explain* brain pathologies. The main limitation for a more extensive use of graph theory is related to non-standardized workflows, e.g., with different graph constructions, thresholds, and, most notably, the lack of practical guidelines on how to interpret the biology behind graph theoretical measures (Onias et al., 2014; Bertolero and Danielle S. Bassett, 2020). The interpretation of certain values is challenging because the MRI processing and the examined disease model must be considered. This makes the establishment of fixed values as generalized indicators or thresholds for determining an unhealthy state difficult. Values cannot be assigned good or bad without any reference. Likewise, the abstraction level of graph theory restricts the judgement whether values at a certain point indicate errors in the analysis.

Currently, there is no generally valid quality control for the analysis with graph theory. In case of bad raw data quality, the high level of abstraction of the underlying data using graph theory will lead to wrong results and misinterpretation - both difficult to detect retrospectively. Like any other advanced analysis technique the abstraction can only be helpful if the raw data is reliable. Research is needed to establish methods to assure the quality of the data. This involves the quality of the recorded raw images to the plausibility of the constructed graphs. Furthermore, research at the cellular or molecular level is needed to establish connections between observed changes in graph theoretical measures and the underlying biological processes. Causal interactions could be investigated by the combination of optogenetic or chemogenetic stimulation and electrophysiological recordings (Desai et al., 2011; Snyder and Bauer, 2019). Functional connectivity measures of cooperation and segregation between brain regions are heavily dependent on the overall network and behavioural state. In addition, altered network states of microcircuits, e.g. the excitatory-to-inhibitory ratio, are causally linked to modulation of functional connectivity (Markicevic et al., 2020). Thus, cross-modality and multiparametric data analysis extending network theory to other in vivo imaging and microscopy techniques with complementary spatiotemporal profile, i.e., optical intrinsic signal imaging, functional ultrasound, and light sheet microscopy is required (White et al., 2011; Tiran et al., 2017; Goubran et al., 2019).

Our summary of current mouse brain MRI studies revealed that the interpretation becomes even more complex when different disease models with different underlying pathologies and time points are studied. In a rapidly developing field, our summary of past studies does not claim to

be complete but provides insight into the large variety of approaches, methods, and interpretations in this field. To stimulate the transition to implement, apply, and interpret network measures, we propose in accordance with recent recommendations for clinical network studies (Hallquist and Hillary, 2018):

1 a harmonized brain parcellation using the Allen Mouse Brain Atlas (CCF v3) with approximately 100 nodes to reduce the variability in topological properties (Zalesky et al., 2010; Pallast, Diedenhofen, et al., 2019; Takata et al., 2021),
2 the documentation and application of standardized pipelines, which have been successfully used for mouse data (e.g. AIDAconnect, CONN, GRETNA or MagnAn),
3 the calculation of a set of network measures, which are combined into more general terms for interpretation (Rubinov and Sporns, 2010), e.g.,
   (a) network segregation (clustering coefficient, modularity, and local efficiency)
   (b) functional integration (characteristic path length and global efficiency)
   (c) network efficiency (small-worldness, shortest path, and global efficiency)
   (d) centrality/hubs (degree/strength, participation coefficient and betweenness centrality)
4 the integration of open science and FAIR data science approaches (Nichols et al., 2017; Borghi and Gulick, 2018) to foster standardized data acquisition, processing, and distribution, as critical elements to develop and advance novel ways to use complex network measures to explain brain function in health and disease in translation mouse brain studies aligned with approaches in human neuroimaging.

Author contributions

Leon Scharwächter: Visualization, Methodology, Writing – Original Draft, Writing – Review & Editing

Felix J. Schmitt: Visualization, Methodology, Writing – Original Draft, Writing – Review & Editing

Niklas Pallast: Conceptualization, Methodology, Writing – Original Draft

Gereon R. Fink: Writing – Original Draft, Writing – Review & Editing, Supervision, Project administration, Funding acquisition

Markus Aswendt: Conceptualization, Supervision, Writing – Original Draft, Writing – Review & Editing, Visualization, Project administration, Funding acquisition

Declarations of Interest

None.

Data and code availability statements: The review summarizes data but does not contain new data.

Acknowledgments

This work was supported by the Friebe Foundation (T0498/28960/16) and the Deutsche Forschungsgemeinschaft (DFG, German Research Foundation) – Project-ID 431549029 – SFB 1451 and 233886668 - GRK1960.

Supplementary materials

Supplementary material associated with this article can be found, in the online version, at doi:10.1016/j.neuroimage.2022.119110.

References

Alexander-Bloch, A.F., Gogtay, N., Meunier, D., Birn, R., Clasen, L., Lalonde, F., Lenroot, R., Giedd, J., Bullmore, E.T., 2010. Disrupted modularity and local connectivity of brain functional networks in childhood-onset schizophrenia. Front. Syst. Neurosci. 4, 147. doi:10.3389/fnsys.2010.00147.

Andica, C., Kamagata, K., Hatano, T., Saito, Y., Ogaki, K., Hattori, N., Aoki, S., 2019. MR biomarkers of degenerative brain disorders derived from diffusion imaging. J. Magn. Reson. Imaging 52 (6), 1620–1636. doi:10.1002/jmri.27019.

Aswendt, M., Green, C., Sadler, R., Llovera, G., Dzikowski, L., Heindl, S., de Agüero, Dieden- hofen, M., Vogel, S., Wieters, F., Wiedermann, D., Liesz, A., Hoehn, M., 2021. The gut microbiota modulates brain network connectivity under physiological conditions and after acute brain ischemia. iScience 24 (10), 103095. doi:10.1016/j.isci.2021.103095.

Aswendt, M., Pallast, N., Wieters, F., Baues, M., Hoehn, M., Fink, G.R., 2020. Lesion size- and location-dependent recruitment of contralesional thalamus and motor cortex facilitates recovery after stroke in mice. Transl. Stroke Res. 12 (1), 87–97. doi:10.1007/s12975-020-00802-3.

Bachmann, C., Jacobs, H.I.L., Mana, P.P., Dillen, K., Richter, N., von Reutern, B., Dronse, J., Onur, O.A., Langen, K.-J., Fink, G.R., Kukolja, J., Morrison, A., 2018. On the extraction and analysis of graphs from resting-state fmri to support a correct and robust diagnostic tool for alzheimer's disease. Front. Neurosci. 12 (528). doi:10.3389/fnins.2018.00528. https://kups.ub.uni-koeln.de/17236/.

Bajaj, S., Adhikari, B.M., Friston, K.J., Dhamala, M., 2016. Bridging the gap: Dynamic causal modeling and granger causality analysis of resting state functional magnetic resonance imaging. Brain Connect. 6 (8), 652–661. doi:10.1089/brain.2016.0422.

Bassett, D.S., Nelson, B.G., Mueller, B.A., Camchong, J., Lim, K.O., 2012. Altered resting state complexity in schizophrenia. Neuroimage 59 (3), 2196–2207. doi:10.1016/j.neuroimage.2011.10.002.

Barbeito-Andrés, J., Gleiser, P.M., Bernal, V., Hallgrímsson, B., Gonzalez, P.N., 2018. Brain structural networks in mouse exposed to chronic maternal undernutrition. Neuroscience 380, 14–26. doi:10.1016/j.neuroscience.2018.03.049.

Benjamini, Y., Hochberg, Y., 1995. Controlling the false discovery rate: A practical and powerful approach to multiple testing. J. R. Stat. Soc. Series B Stat. Methodol. 57 (1), 289–300. doi:10.1111/j.2517-6161.1995.tb02031.x.

Berlot, R., Metzler-Baddeley, C., Ikram, M.A., Jones, D.K., O'Sullivan, M.J, 2016. Global efficiency of structural networks mediates cognitive control in mild cognitive impairment. Front. Aging Neurosci. 08. doi:10.3389/fnagi.2016.00292.

Bertolero, M.A., Bassett, D.S., 2020. On the nature of explanations offered by network science: A perspective from and for practicing neuroscientists. Top. Cogn. Sci. 12 (4), 1272–1293. doi:10.1111/tops.12504.

Bifone, A., Gozzi, A., Schwarz, A.J., 2010. Functional connectivity in the rat brain: A complex network approach. Magn. Reson. Imaging 28 (8), 1200–1209. doi:10.1016/j.mri.2010.07.00.

Blaschke, S.J., Hensel, L., Minassian, A., Vlachakis, S., Tscherpel, C., Vay, S.U., Rabenstein, M., Schroeter, M., Fink, G.R., Hoehn, M., Grefkes, C., Rueger, M.A., 2021. Translating func- tional connectivity after stroke: Functional magnetic resonance imaging detects comparable net- work changes in mice and humans. Stroke 52 (9), 2948–2960. doi:10.1161/strokeaha.120.032511.

Blondel, V.D., Guillaume, J.-L., Lambiotte, R., Lefebvre, E., 2008. Fast unfolding of communities in large networks. J. Stat. Mech. Theory Exp. 2008 (10), P10008. doi:10.1088/1742-5468/2008/10/p10008.

Boehm-Sturm, P., Füchtemeier, M., Foddis, M., Mueller, S., Trueman, R.C., Zille, M., Rinnenthal, L., Kypraios, T., Shaw, L., Dirnagl, U., Farr, T.D., 2017. Neuroimaging biomarkers predict brain structural connectivity change in a mouse model of vascular cognitive impairment. Stroke 48 (2), 468–475. doi:10.1161/strokeaha.116.014394.

Boretius, S., Würfel, J., Zipp, F., Frahm, J., Michaelis, T., 2007. High-field diffusion tensor imaging of mouse brain in vivo using single-shot STEAM MRI. J. Neurosci. Methods 161 (1), 112–117. doi:10.1016/j.jneumeth.2006.10.019.

Borghi, J.A., Gulick, A.E.V., 2018. Data management and sharing in neuroimaging: Practices and perceptions of MRI researchers. PLoS One 13 (7), e0200562. doi:10.1371/journal.pone.0200562.

Buchanan, C.R., Bastin, M.E., Ritchie, S.J., Liewald, D.C., Madole, J.W., Tucker-Drob, E.M., Deary, I.J., Cox, S.R., 2020. The effect of network thresholding and weighting on structural brain networks in the UK biobank. Neuroimage 211, 116443. doi:10.1016/j.neuroimage, 2019.116443.

Bukhari, Q., Schroeter, A., Cole, D.M., Rudin, M., 2017. Resting state fMRI in mice reveals anes- thesia specific signatures of brain functional networks and their interactions. Front. Neural Circuits 11. doi:10.3389/fncir.2017.00005.

Bullmore, E., Sporns, O., 2009. Complex brain networks: Graph theoretical analysis of structural and functional systems. Nat. Rev. Neurosci. 10 (3), 186–198. doi:10.1038/nrn2575.

Calabrese, E., Badea, A., Cofer, G., Qi, Y., Johnson, G.A., 2015. A diffusion MRI tractography connectome of the mouse brain and comparison with neuronal tracer data. Cereb. Cortex 25 (11), 4628–4637. doi:10.1093/cercor/bhv121.

Cerina, M., Muthuraman, M., Gallus, M., Koirala, N., Dik, A., Wachsmuth, L., Hundehege, P., Schiffler, P., Tenberge, 0.-G., Fleischer, V., Gonzalez-Escamilla, G., Narayanan, V., Krämer, 0., Faber, C., Budde, T., Groppa, S., Meuth, S.G., 2020. Myelination- and immune-mediated MR-based brain network correlates. J. Neuroinflammation 17 (1). doi:10.1186/s12974-020-01827-z.

Chon, U., Vanselow, D.J., Cheng, K.C., Kim, Y., 2019. Enhanced and unified anatomical labeling for a common mouse brain atlas. Nat. Commun. 10 (1). doi:10.1038/s41467-019-13057-w.

Coletta, L., Pagani, M., Whitesell, J.D., Harris, 0.A., Bernhardt, B., Gozzi, A., 2020. Network struc- ture of the mouse brain connectome with voxel resolution. Sci. Adv. 6 (51). doi:10.1126/sciadv.abb7187, eabb7187.

Colon-Perez, L.M., Ibanez, K.R., Suarez, M., Torroella, K., Acuna, K., Ofori, E., Levites, Y., Vaillan- court, D.E., Golde, T.E., Chakrabarty, P., Febo, M., 2019. Neurite orientation dispersion and density imaging reveals white matter and hippocampal microstructure changes produced by interleukin-6 in the TgCRND8 mouse model of amyloidosis. Neuroimage 202, 116138. doi:10.1016/j.neuroimage.2019.116138.

Conti, A., Duggento, A., Guerrisi, M., Passamonti, L., Indovina, I., Toschi, N., 2019. Variability and reproducibility of directed and undirected functional mri connectomes in the human brain. Entropy 21 (7). doi:10.3390/e21070661.

Crofts, J., Higham, D., Bosnell, R., Jbabdi, S., Matthews, P., Behrens, T., Johansen-Berg, H., 2011. Network analysis detects changes in the contralesional hemisphere following stroke. Neuroimage 54 (1), 161–169. doi:10.1016/j.neuroimage.2010.08.032.

Desai, M., Kahn, I., Knoblich, U., Bernstein, J., Atallah, H., Yang, A., Kopell, N., Buckner, R.L., Graybiel, A.M., Moore, C.I., Boyden, E.S., 2011. Mapping brain networks in awake mice using combined optical neural control and fMRI. J. Neurophysiol. 105 (3), 1393–1405. doi:10.1152/jn.00828.2010.

Dorr, A., Lerch, J., Spring, S., Kabani, N., Henkelman, R., 2008. High resolution three-dimensional brain atlas using an average magnetic resonance image of 40 adult c57bl/6j mice. Neuroimage 42 (1), 60–69. doi:10.1016/j.neuroimage.2008.03.037.

Fallani, F.D.V., Richiardi, J., Chavez, M., Achard, S., 2014. Graph analysis of functional brain networks: Practical issues in translational neuroscience. Philos. Trans. R. Soc. B: Biol. Sci. 369 (1653), 20130521. doi:10.1098/rstb.2013.0521.

Farahani, F.V., Karwowski, W., Lighthall, N.R., 2019. Application of graph theory for identifying connectivity patterns in human brain networks: A systematic review. Front. Neurosci. 13. doi:10.3389/fnins.2019.00585.

Fernández-García, S., Conde-Berriozabal, S., García-García, E., Gort-Paniello, C., Bernal-Casas, D., García-Díaz Barriga, G., López-Gil, J., Muñoz-Moreno, E., Soria, G., Campa, L., Artigas, F., Rodríguez, M. J., Alberch, J., Masana, M., 2020. M2 cortex-dorsolateral striatum stimulation reverses motor symptoms and synaptic deficits in Huntington's disease. eLife 9, e57017. doi:10.7554/eLife.57017.

Fornito, A., Zalesky, A., Bullmore, E.T., 2016. Fundamentals of brain network analysis. Elsevier doi:10.1016/c2012-0-06036-x.

Franklin, K.B., Paxinos, G., 2008. The mouse brain in stereotaxic coordinates, compact: The coronal plates and diagrams, (third ed.) Academic Press.

Garrison, K.A., Scheinost, D., Finn, E.S., Shen, X., Constable, R.T., 2015. The (in)stability of functional brain network measures across thresholds. Neuroimage 118, 651–661. doi:10.1016/j.neuroimage.2015.05.046.

Good, P., 1994. Permutation tests. Springer, New York https://doi.org/10.1007/978-1-4757-2346-5.

Gorges, 0., Roselli, F., Müller, H.-P., Ludolph, A.C., Rasche, V., Kassubek, 0., 2017. Functional connectivity mapping in the animal model: Principles and applications of resting-state fMRI. Front. Neurol. 8 (200). doi:10.3389/fneur.2017.00200.

Goubran, M., Leuze, C., Hsueh, B., Aswendt, M., Ye, L., Tian, Q., Cheng, M.Y., Crow, A., Steinberg, G.K., McNab, J.A., Deisseroth, K., Zeineh, M., 2019. Multimodal image registration and connectivity analysis for integration of connectomic data from microscopy to MRI. Nat. Commun. (1) 10. doi:10.1038/s41467-019-13374-0.

Grandjean, J., Canella, C., Anckaerts, C., Ayrancı, G., Bougacha, S., Bienert, T., Buehlmann, D., Coletta, L., Gallino, D., Gass, N., Garin, C.M., Nadkarni, N.A., Hübner, N.S., Karatas, M., Komaki, Y., Kreitz, S., Mandino, F., Mechling, A.E., Sato, C., Sauer, K., Gozzi, A., 2020. Common functional networks in the mouse brain revealed by multi-centre resting-state fMRI analysis. Neuroimage 205, 116278. doi:10.1016/j.neuroimage.2019.116278.

Grandjean, J., Schroeter, A., Batata, I., Rudin, M., 2014. Optimization of anesthesia protocol for resting-state fMRI in mice based on differential effects of anesthetics on functional connectivity patterns. Neuroimage 102, 838–847. doi:10.1016/j.neuroimage.2014.08.043.

Grandjean, J., Zerbi, V., Balsters, J.H., Wenderoth, N., Rudin, M., 2017. Structural basis of large- scale functional connectivity in the mouse. J. Neurosci. 37 (34), 8092–8101. doi:10.1523/jneurosci.0438-17.2017.

Green, C., Minassian, A., Vogel, S., Diedenhofen, M., Beyrau, A., Wiedermann, D., Hoehn, M., 2018. Sensorimotor functional and structural networks after intracerebral stem cell grafts in the is- chemic mouse brain. The Journal of Neuroscience 38 (7), 1648–1661. doi:10.1523/jneurosci.2715-17.2018.

Grefkes, C., Fink, G.R., 2014. Connectivity-based approaches in stroke and recovery of function. The Lancet Neurology 13 (2), 206–216. doi:10.1016/s1474-4422(13)70264-3.

Guimerà, R., Amaral, L.A.N., 2005. Cartography of complex networks: Modules and universal roles. J. Stat. Mech. Theory Exp. 2005 (P02001), nihpa35573. doi:10.1088/1742-5468/2005/02/p02001.

Hallquist, M.N., Hillary, F.G., 2018. Graph theory approaches to functional network organization in brain disorders: A critique for a brave new small-world. Netw. Neurosci. 3 (1), 1–26. doi:10.1162/netn_a_00054.

Harsan, L.-A., David, C., Reisert, M., Schnell, S., Hennig, J., von Elverfeldt, D., Staiger, J.F., 2013. Mapping remodeling of thalamocortical projections in the living reeler mouse brain by diffusion tractography. Proc. Natl. Acad. Sci. 110 (19), E1797–E1806. doi:10.1073/pnas.1218330110.

Hawrylycz, M., Baldock, R.A., Burger, A., Hashikawa, T., Johnson, G.A., Martone, M., Ng, L., Lau, C., Larsen, S.D., Nissa11, J., Puelles, L., Ruffins, S., Verbeek, F., Zaslavsky, I., Boline, J., 2011. Digital atlasing and standardization in the mouse brain (L. J. Graham, Ed.). PLoS Comput. Biol. 7 (2), e1001065. doi:10.1371/journal.pcbi.1001065.

He, Y., Dagher, A., Chen, Z., Charil, A., Zijdenbos, A., Worsley, K., Evans, A., 2009. Impaired small- world efficiency in structural cortical networks in multiple sclerosis associated with white matter lesion load. Brain 132 (12), 3366–3379. doi:10.1093/brain/awp089.

Hess, A., Hinz, R., Keliris, G.A., Boehm-Sturm, P., 2018. On the usage of brain atlases in neuroimag- ing research. Mol. Imaging Biol. 20 (5), 742–749. doi:10.1007/s11307-018-1259-y.

Hilgetag, C.C., Goulas, A., 2015. Is the brain really a small-world network? Brain Struct. Funct. 221 (4), 2361–2366. doi:10.1007/s00429-015-1035-6.

Himberg, J., Hyv¨arinen, A., Esposito, F., 2004. Validating the independent components of neu- roimaging time series via clustering and visualization. Neuroimage 22 (3), 1214–1222. doi:10.1016/j.neuroimage.2004.03.027.

Hoehn, M., Aswendt, M., 2013. Structure–function relationship of cerebral networks in experimental neuroscience: Contribution of magnetic resonance imaging. Exp. Neurol. 242, 65–73. doi:10.1016/j.expneurol.2012.04.014.

Horn, A., Fox, M.D., 2020. Opportunities of connectomic neuromodulation. Neuroimage 221, 117180. doi:10.1016/j.neuroimage.2020.117180.

Hübner, N.S., Mechling, A.E., Lee, H.-L., Reisert, M., Bienert, T., Hennig, J., von Elverfeldt, D., Harsan, L.-A., 2017. The connectomics of brain demyelination: Functional and structural patterns in the cuprizone mouse model. Neuroimage 146, 1–18. doi:10.1016/j.neuroimage.2016.11.008.

Iturria-Medina, Y., Ontivero-Ortega, M., Canales-Rodríguez, E.J., Melie-García, L., Valdés-Hernández, P., Pérez-Fernández, A., 2013. Complex Mouse Brain Anatomical Network Attributes Estimated via Diffusion- MRI Data and Graph Theory. In: Folgueras Méndez, J. (Ed.), V Latin American Congress on Biomedical Engineering CLAIB 2011 May 16-21, 2011, Habana, Cuba. Springer, Berlin Heidelberg, pp. 65–68 https://doi.org/10.1007/978-3-642-21198-0 17.

Janke, A.L., Ullmann, J.F., 2015. Robust methods to create ex vivo minimum deformation atlases for brain mapping. Methods 73, 18–26. doi:10.1016/j.ymeth.2015.01.005.

Johnson, G.A., Badea, A., Brandenburg, J., Cofer, G., Fubara, B., Liu, S., Nissa11, J., 2010. Waxholm space: An image-based reference for coordinating mouse brain research. Neuroimage 53 (2), 365–372. doi:10.1016/j.neuroimage.2010.06.067.

Jonckers, E., Shah, D., Hamaide, 0., Verhoye, M., der Linden, A.V., 2015. The power of using functional fMRI on small rodents to study brain pharmacology and disease. Front. Pharmacol. 6. doi:10.3389/fphar.2015.00231.

Jones, T.A., Adkins, D.L., 2015. Motor system reorganization after stroke: Stimulating and training toward perfection. Physiology 30 (5), 358–370. doi:10.1152/physiol.00014.2015.

Kalthoff, D., Seehafer, J.U., Po, C., Wiedermann, D., Hoehn, M., 2011. Functional connectivity in the rat at 11.7t: Impact of physiological noise in resting state fMRI. Neuroimage 54 (4), 2828–2839. doi:10.1016/j.neuroimage.2010.10.053.

Karatas, M., Noblet, V., Nasseef, M.T., Bienert, T., Reisert, M., Hennig, J., Yalcin, I., Kieffer, B.L., von Elverfeldt, D., Harsan, L.-A., 2021. Mapping the living mouse brain neural architec- ture: Strain-specific patterns of brain structural and functional connectivity. Brain Struct. Funct. 226 (3), 647–669. doi:10.1007/s00429-020-02190-8.

Kim, J., Wozniak, J.R., Mueller, B.A., Shen, X., Pan, W., 2014. Comparison of statistical tests for group differences in brain functional networks. Neuroimage 101, 681–694. doi:10.1016/j.neuroimage.2014.07.031.

Kleinberg, J.M., 1999. Hubs, authorities, and communities. ACM computing surveys 31 (4es). doi:10.1145/345966.345982, 5–es.

Knox, J.E., Harris, K.1., Graddis, N., Whitesell, J.D., Zeng, H., Harris, 0.A., Shea-Brown, E., Mihalas, S., 2019. High-resolution data-driven model of the mouse connectome. Netw. Neurosci. 3 (1), 217–236. doi:10.1162/netn_a_00066.eCollection 2019.

Koch, S., Müller, S., Foddis, M., Bienert, T., von Elverfeldt, D., Knab, F., Farr, T.D., Bernard, R., Dopatka, M., Rex, A., Dirnagl, U., Harms, C., Boehm-Sturm, P., 2017. Atlas registration for edema-corrected MRI lesion volume in mouse stroke models. J. CEREBR. BLOOD F. MET. 39 (2), 313–323. doi:10.1177/0271678x17726635.

Komaki, Y., Hikishima, K., Shibata, S., Konomi, T., Seki, F., Yamada, M., Miyasaka, N., Fujiyoshi, K., Okano, H.J., Nakamura, M., Okano, H., 2016. Functional brain mapping using specific sensory-circuit stimulation and a theoretical graph network analysis in mice with neuropathic allodynia. Sci. Rep. 6 (1). doi:10.1038/srep37802.

Kreitz, S., Zambon, A., Ro11sky, M., Budinsky, L., Helbich, T.H., Sideromenos, S., Ivan, C., Konerth, L., Wank, I., Berger, A., et al., 2020. Maternal immune activation during pregnancy impacts on brain structure and function in the adult offspring. Brain Behav. Immun. 83, 56–67. doi:10.1016/j.bbi.2019.09.011.

Lawrence, A.J., Chung, A.W., Morris, R.G., Markus, H.S., Barrick, T.R., 2014. Structural network efficiency is associated with cognitive impairment in small-vessel disease. Neurology 83 (4), 304–311. doi:10.1212/wnl.0000000000000612.

Lein, E.S., Hawrylycz, M.J., Ao, N., Ayres, M., Bensinger, A., Bernard, A., Boe, A.F., Boguski, M.S., Brockway, K.S., Byrnes, E.J., Chen, L., Chen, L., Chen, T.-M., Chin, M.C., Chong, J., Crook, B.E., Czaplinska, A., Dang, C.N., Datta, S., Dee, N.R., Jones, A.R., 2007. Genome-wide atlas of gene expression in the adult mouse brain. Nature 445 (7124), 168–176. doi:10.1038/nature05453.

Liska, A., Galbusera, A., Schwarz, A.J., Gozzi, A., 2015. Functional connectivity hubs of the mouse brain. Neuroimage 115, 281–291. doi:10.1016/j.neuroimage.2015.04.033.

Liu, C., Li, Y., Edwards, T.J., Kurniawan, N.D., Richards, L.J., Jiang, T., 2016. Altered structural connectome in adolescent socially isolated mice. Neuroimage 139, 259–270. doi:10.1016/j.neuroimage.2016.06.037.

Lohse, C., Bassett, D.S., Lim, K.O., Carlson, J.M., 2014. Resolving anatomical and functional structure in human brain organization: Identifying mesoscale organization in weighted network representations. PLoS Comput. Biol. 10 (10), 1–17. doi:10.1371/journal. pcbi.1003712.

Luppi, A.I., Stamatakis, E.A., 2021. Combining network topology and information theory to construct representative brain networks. Netw. Neurosci. 5 (1), 96–124. doi:10.1162/netna_00170.eCollection2021.

Ma, D., Cardoso, M.J., Modat, M., Powell, N., Wells, J., Holmes, H., Wiseman, F., Tybulewicz, V., Fisher, E., Lythgoe, M.F., Ourselin, S., 2014. Automatic structural parcellation of mouse brain MRI using multi-atlas label fusion. PLoS One 9 (1), e86576. doi:10.1371/journal.pone.0086576.

Ma, Y., Hof, P., Grant, S., Blackband, S., Bennett, R., Slatest, L., McGuigan, M., Benveniste, H, 2005. A three-dimensional digital atlas database of the adult C57BL/6J mouse brain by magnetic resonance microscopy. Neuroscience 135 (4), 1203–1215 https://doi.org/10.1016/j.neuroscience. 2005.07.014.

Ma, Y., Smith, D., Hof, P.R., Foerster, B., Hamilton, S., Blackband, S.J., Yu, M., Benveniste, H., 2008. In vivo 3D digital atlas database of the adult C57Bl/6J mouse brain by magnetic resonance microscopy. Front. Neuroanat. 2 (1). doi:10.3389/neuro.05.001.2008.

MacKenzie-Graham, A.J., Lee, E.-F., Dinov, I.D., Yuan, H., Jacobs, R.E., Toga, A.W., 2007. Multimodal, multidimensional models of mouse brain. Epilepsia 48 (s4), 75–81. doi:10.1111/j.1528-1167.2007.01244.x.

Mandino, F., Cerri, D.H., Garin, C.M., Straathof, M., van Tilborg, G.A.F., Chakravarty, M.M., Dhenain, M., Dijkhuizen, R.M., Gozzi, A., Hess, A., Keilholz, S.D., Lerch, J.P., Shih, Y.-Y.I., Grandjean, J., 2020. Animal functional magnetic resonance imaging: Trends and path toward standardization. Front. Neuroinform. 13. doi:10.3389/fninf.2019.00078.

Markicevic, M., Fulcher, B.D., Lewis, C., Helmchen, F., Rudin, M., Zerbi, V., Wenderoth, N., 2020. Cortical Excitation:Inhibition Imbalance Causes Abnormal Brain Network Dynamics as Observed in Neurodevelopmental Disorders. Cereb. Cortex 30 (9), 4922–4937. doi:10.1093/cercor/bhaa084.

Mazziotta, J., Ioga, A., Evans, A., Fox, P., Lancaster, J., Zilles, K., Woods, R., Paus, T., Simpson, G., Pike, B., Holmes, C., Collins, L., Thompson, P., MacDonald, D., Iacoboni, M., Schormann, T., Amunts, K., Palomero-Gallagher, N., Geyer, S., Parsons, L., … Mazoyer, B., 2001. A probabilistic atlas and reference system for the human brain: International Consortium for Brain Mapping (ICBM). Philos. Trans. R. Soc. B: Biol. Sci. 356 (1412), 1292–1322 doi:10.1098/rstb.2001.0915.

Mechling, A.E., Arefin, T., Lee, H.-L., Bienert, T., Reisert, M., Hamida, S.B., Darcq, E., Ehrlich, A., Gaveriaux-Ruff, C., Parent, M.J., Rosa-Neto, P., Hennig, J., von Elverfeldt, D., Kieffer, B.L., Harsan, L.-A., 2016. Deletion of the mu opioid receptor gene in mice reshapes the reward–aversion connectome. Proc. Natl. Acad. Sci. 113 (41), 11603–11608. doi:10.1073/pnas.1601640113.

Mechling, A.E., Hübner, N.S., Lee, H.-L., Hennig, J., von Elverfeldt, D., Harsan, L.-A., 2014. Fine-grained mapping of mouse brain functional connectivity with resting-state fMRI. Neuroimage 96, 203–215. doi:10.1016/j.neuroimage.2014.03.078.

Melozzi, F., Bergmann, E., Harris, 0.A., Kahn, I., Jirsa, V., Bernard, C., 2019. Individual structural features constrain the mouse functional connectome. Proc. Natl. Acad. Sci. 116 (52), 26961–26969. doi:10.1073/pnas.1906694116.

Meningher, I., Bernstein-Eliav, M., Rubovitch, V., Pick, C.G., Tavor, I., 2020. Alterations in network connectivity after traumatic brain injury in mice. J. Neurotrauma 37 (20), 2169–2179. doi:10.1089/neu.2020.7063.

Mills, B.D., Grayson, D.S., Shunmugavel, A., Miranda-Dominguez, O., Feczko, E., Earl, E., Neve, K.A., Fair, D.A., 2018. Correlated gene expression and anatomical communication support synchronized brain activity in the mouse functional connectome. J. Neurosci. 38 (25), 5774–5787. doi:10.1523/jneurosci.2910-17.2018.

Müller, H.-P., Roselli, F., Rasche, V., Kassubek, 0, 2020. Diffusion tensor imaging-based studies at the group-level applied to animal models of neurodegenerative diseases. Front. Neurosci. 14. doi:10.3389/fnins.2020.00734.

Newman, M.E.J., 2006. Modularity and community structure in networks. Proc. Natl. Acad. Sci. 103 (23), 8577–8582. doi:10.1073/pnas.0601602103.

Nichols, T.E., Das, S., Eickhoff, S.B., Evans, A.C., Glatard, T., Hanke, M., Kriegeskorte, N., Milham, M.P., Poldrack, R.A., Poline, J.-B., Proal, E., Thirion, B., Essen, D.C.V., White, T., Yeo, B.T.T, 2017. Best practices in data analysis and sharing in neuroimaging using MRI. Nat. Neurosci. 20 (3), 299–303. doi:10.1038/nn.4500.

Oh, S.W., Harris, J.A., Ng, L., Winslow, B., Cain, N., Mihalas, S., Wang, Q., Lau, C., Kuan, L., Henry, A.M., Mortrud, M.T., Ouellette, B., Nguyen, T.N., Sorensen, S.A., Slaughterbeck, C.R., Wakeman, W., Li, Y., Feng, D., Ho, A., Nicholas, E., Zeng, H., 2014. A mesoscale connectome of the mouse brain. Nature 508 (7495), 207–214. doi:10.1038/nature13186.

Onias, H., Viol, A., Palhano-Fontes, F., Andrade, K.C., Sturzbecher, M., Viswanathan, G., de Araujo, D.B., 2014. Brain complex network analysis by means of resting state fMRI and graph analysis: Will it be helpful in clinical epilepsy? Epilepsy Behav. 38, 71–80. doi:10.1016/j.yebeh.2013.11.019.

Pallast, N., Diedenhofen, M., Blaschke, S., Wieters, F., Wiedermann, D., Hoehn, M., Fink, G.R., Aswendt, M., 2019. Processing pipeline for atlas-based imaging data analysis of structural and functional mouse brain MRI (AIDAmri). Front. Neuroinform. 13. doi:10.3389/fninf.2019.00042.

Pallast, N., Wieters, F., Nill, M., Fink, G.R., Aswendt, M., 2020. Graph theoretical quantification of white matter reorganization after cortical stroke in mice. Neuroimage 217, 116873. doi:10.1016/j.neuroimage.2020.116873.

Pan, W.-J., Billings, J.C.W., Grooms, J.K., Shakil, S., Keilholz, S.D., 2015. Considerations for resting state functional MRI and functional connectivity studies in rodents. Front. Neurosci. 9. doi:10.3389/fnins.2015.00269.

Peeters, L.M., Hinz, R., Detrez, 0.R., Missault, S., Vos, W.H.D., Verhoye, M., der Linden, A.V., Keliris, G.A., 2020. Chemogenetic silencing of neurons in the mouse anterior cingulate area modulates neuronal activity and functional connectivity. Neuroimage 220, 117088. doi:10.1016/j.neuroimage.2020.117088.

Pierpaoli, C., Basser, P.J., 1996. Toward a quantitative assessment of diffusion anisotropy. Magn. Reson. Med. 36 (6), 893–906. doi:10.1002/mrm.1910360612.

Pradier, B., Wachsmuth, L., Nagelmann, N., Segelcke, D., Kreitz, S., Hess, A., Pogatzki-Zahn, E.M., Faber, C., 2021. Combined resting state-fMRI and calcium recordings show stable brain states for task-induced fMRI in mice under combined ISO/MED anesthesia. Neuroimage 245, 118626. doi:10.1016/j.neuroimage.2021.118626.

Rubinov, M., Sporns, O., 2010. Complex network measures of brain connectivity: Uses and interpre- tations. Neuroimage 52 (3), 1059–1069. doi:10.1016/j.neuroimage.2009.10.003.

Ryali, S., Shih, Y.-Y.I., Chen, T., Kochalka, J., Albaugh, D., Fang, Z., Supekar, K., Lee, J.H., Menon, V., 2016. Combining optogenetic stimulation and fMRI to validate a multivariate dynamical systems model for estimating causal brain interactions. Neuroimage 132, 398–405. doi:10.1016/j.neuroimage.2016.02.067.

Sethi, S. S., Zerbi, V., Wenderoth, N., Fornito, A., Fulcher, B. D., 2016. Structural connectome topology relates to regional BOLD signal dynamics in the mouse brain. Chaos 27 (4), 047405. doi:10.1101/085514.

Snyder, A.Z., Bauer, A.Q., 2019. Mapping structure-function relationships in the brain. Biol. Psychiatry: Cogn. Neurosci. Neuroimaging 4 (6), 510–521. doi:10.1016/j.bpsc.2018.10.005.

Sporns, O., 2010. Networks of the brain. Networks of the brain.. The MIT Press, Cambridge https://doi.org/10.7551/mitpress/8476.001. 0001.

Sporns, O., Bullmore, E.T., 2014. From connections to function: The mouse brain connectome atlas. Cell 157 (4), 773–775. doi:10.1016/j.cell.2014.04.023.

Stam, C., Jones, B., Nolte, G., Breakspear, M., Scheltens, P., 2006. Small-World Networks and Functional Connectivity in Alzheimer's Disease. Cereb. Cortex 17 (1), 92–99. doi:10.1093/cercor/bhj127.

Stouffer, S.A., 1936. Reliability coefficients in a correlation matrix. Psychometrika 1 (2), 17–20. doi:10.1007/bf02288001.

Straathof, M., Sinke, M.R.T., Roelofs, T.J.M., Blezer, E.L.A., Sarabdjitsingh, R.A., van der Toorn, A., Schmitt, O., Otte, W.M., Dijkhuizen, R.M., 2020. Distinct structure-function relationships across cortical regions and connectivity scales in the rat brain. Sci. Rep. (1) 10. doi:10.1038/s41598-019-56834-9.

Takata, N., Sato, N., Komaki, Y., Okano, H., Tanaka, K.F., 2021. Flexible annotation atlas of the mouse brain: Combining and dividing brain structures of the allen brain atlas while maintaining anatomical hierarchy. Sci. Rep. (1) 11. doi:10.1038/s41598-021-85807-0.

Tiran, E., Ferrier, J., Deffieux, T., Gennisson, J.-L., Pezet, S., Lenkei, Z., Tanter, M., 2017. Tran- scranial functional ultrasound imaging in freely moving awake mice and anesthetized young rats without contrast agent. Ultrasound Med. Biol. 43 (8), 1679–1689. doi:10.1016/j.ultrasmedbio.2017.03.011.

Tsurugizawa, T., Tamada, K., Ono, N., Karakawa, S., Kodama, Y., Debacker, C., Hata, J., Okano, H., Kitamura, A., Zalesky, A., Takumi, T., 2020. Awake functional MRI detects neural circuit dysfunction in a mouse model of autism. Sci. Adv. (6) 6. doi:10.1126/sciadv.aav4520.

van den Heuvel, M.P., de Lange, S.C., Zalesky, A., Seguin, C., Yeo, B.T., Schmidt, R., 2017. Pro- portional thresholding in resting-state fMRI functional connectivity networks and consequences for patient-control connectome studies: Issues and recommendations. Neuroimage 152, 437–449. doi:10.1016/j.neuroimage.2017.02.005.

van den Heuvel, M.P., Pol, H.E.H., 2010. Exploring the brain network: A review on resting-state fMRI functional connectivity. Eur. Neuropsychopharmacol. 20 (8), 519–534. doi:10.1016/j.euroneuro.2010.03.008.

van den Heuvel, M.P., Sporns, O., 2013. Network hubs in the human brain. Trends Cogn. Sci. 17 (12), 683–696. doi:10.1016/j.tics.2013.09.012.

van den Heuvel, M.P., Sporns, O., 2019. A cross-disorder connectome landscape of brain dysconnectivity. Nat. Rev. Neurosci. 20 (7), 435–446. doi:10.1038/s41583-019-0177-6.

van Meer, M.P.A., Otte, W.M., van der Marel, K., Nijboer, C.H., Kavelaars, A., van der Sprenkel, J.W.B., Viergever, M.A., Dijkhuizen, R.M., 2012. Extent of bilateral neuronal network reorganization and functional recovery in relation to stroke severity. J. Neurosci. 32 (13), 4495–4507. doi:10.1523/jneurosci.3662-11.2012.

van Wijk, B.C.M., Stam, C.J., Daffertshofer, A., 2010. Comparing brain networks of different size and connectivity density using graph theory (O. Sporns, Ed.). PLoS One 5 (10), e13701. doi:10.1371/journal.pone.0013701.

Wang, H.E., Bénar, C.G., Quilichini, P.P., Friston, K.J., Jirsa, V.K., Bernard, C, 2014. A systematic framework for functional connectivity measures. Front. Neurosci. 8, 405. doi:10.3389/fnins.2014.00405.

Wang, J., Wang, X., Xia, M., Liao, X., Evans, A., He, Y., 2015. GRETNA: A graph theoretical network analysis toolbox for imaging connectomics. Front. Hum. Neurosci. 9. doi:10.3389/fnhum.2015.00386.

Wang, Q., Ding, S.-L., Li, Y., Royall, J., Feng, D., Lesnar, P., Graddis, N., Naeemi, M., Facer, B., Ho, A., Dolbeare, T., Blanchard, B., Dee, N., Wakeman, W., Hirokawa, K.E., Szafer, A., Sunkin, S.M., Oh, S.W., Bernard, A., Phillips, J.W., … Ng, L., 2020. The allen mouse brain common coordinate framework: A 3d reference atlas. *Cell* 181 (4). doi:10.1016/j.cell.2020.04.007, 936–953.e20.

White, B.R., Bauer, A.Q., Snyder, A.Z., Schlaggar, B.L., Lee, J.-M., Culver, J.P., 2011. Imaging of functional connectivity in the mouse brain (O. Sporns, Ed.). PLoS One 6 (1), e16322. doi:10.1371/journal.pone.0016322.

Whitfield-Gabrieli, S., Nieto-Castanon, A., 2012. Conn: A functional connectivity toolbox for corre- lated and anticorrelated brain networks. Brain Connect. 2 (3), 125–141. doi:10.1089/brain.2012.0073.

Yoshida, K., Mimura, Y., Ishihara, R., Nishida, H., Komaki, Y., Minakuchi, T., Tsurugizawa, T., Mimura, M., Okano, H., Tanaka, K.F., Takata, N., 2016. Physiological effects of a habituation proce- dure for functional mri in awake mice using a cryogenic radiofrequency probe. J Neurosci. Meth. 274, 38–48. doi:10.1016/j.jneumeth.2016.09.013.

Zalesky, A., Fornito, A., Harding, I.H., Cocchi, L., Yu¨cel, M., Pantelis, C., Bullmore, E.T., 2010. Whole-brain anatomical networks: Does the choice of nodes matter? Neuroimage 50 (3), 970–983. doi:10.1016/j.neuroimage.2009.12.027.

Zalesky, A., Fornito, A., Seal, M.L., Cocchi, L., Westin, C.-F., Bullmore, E.T., Egan, G.F., Pantelis, C., 2011. Disrupted axonal fiber connectivity in schizophrenia. Biol. Psychiatry 69 (1), 80–89. doi:10.1016/j.biopsych.2010.08.022.

Zerbi, V., Grandjean, J., Rudin, M., Wenderoth, N., 2015. Mapping the mouse brain with rs-fMRI: An optimized pipeline for functional network identification. Neuroimage 123, 11–21. doi:10.1016/j.neuroimage.2015.07.090.